



# Canadian Journal of Remote Sensing

## Journal canadien de télédétection

ISSN: 0703-8992 (Print) 1712-7971 (Online) Journal homepage: <https://www.tandfonline.com/loi/ujrs20>

## Ozone Measurements Using the Refurbished Eureka Stratospheric Differential Absorption Lidar

Alexey B. Tikhomirov, Ghazal Farhani, Emily M. McCullough, Robert J. Sica, Pierre F. Fogal, Thierry Leblanc & James R. Drummond

To cite this article: Alexey B. Tikhomirov, Ghazal Farhani, Emily M. McCullough, Robert J. Sica, Pierre F. Fogal, Thierry Leblanc & James R. Drummond (2019): Ozone Measurements Using the Refurbished Eureka Stratospheric Differential Absorption Lidar, Canadian Journal of Remote Sensing, DOI: [10.1080/07038992.2019.1651195](https://doi.org/10.1080/07038992.2019.1651195)

To link to this article: <https://doi.org/10.1080/07038992.2019.1651195>



Published online: 24 Aug 2019.



Submit your article to this journal [↗](#)



Article views: 35




View related articles [↗](#)



View Crossmark data [↗](#)



## Ozone Measurements Using the Refurbished Eureka Stratospheric Differential Absorption Lidar

Alexey B. Tikhomirov<sup>a</sup>, Ghazal Farhani<sup>b</sup>, Emily M. McCullough<sup>a</sup>, Robert J. Sica<sup>b</sup> , Pierre F. Fogal<sup>c</sup>, Thierry Leblanc<sup>d</sup>, and James R. Drummond<sup>a</sup>

<sup>a</sup>Department of Physics and Atmospheric Science, Dalhousie University, Halifax, NS, Canada; <sup>b</sup>Department of Physics and Astronomy, The University of Western Ontario, London, ON, Canada; <sup>c</sup>Department of Physics, University of Toronto, Toronto, ON, Canada; <sup>d</sup>Jet Propulsion Laboratory, California Institute of Technology, Wrightwood, CA, USA

### ABSTRACT

The Stratospheric Ozone Differential Absorption Lidar (DIAL) located at the Polar Environment Atmospheric Research Laboratory (PEARL) in Eureka, Nunavut (80°N, 86°W) has been a powerful tool for the measurement of stratospheric ozone vertical profiles in the Canadian High Arctic since 1993. The lidar ozone profiles measured during the 2017 Canadian Arctic Atmospheric Chemistry Experiment (ACE) and Optical Spectrograph and InfraRed Imaging System (OSIRIS) Validation Campaign were compared to coincident ozonesonde, ACE-FTS, ACE-MAESTRO and OSIRIS profiles. The results show the lidar overestimates the ozone by ~10% in the 10 km–20 km altitude range on average in comparison with the ozonesonde. Above 20 km the profiles agree within 10%. The OSIRIS ozone agrees within 10% with DIAL ozone between 15 km and 41 km. A strong stratospheric ozone depletion event was seen on March 3, 2017, during which the ozone concentration dropped below  $10^{12}$  molecules  $\text{cm}^{-3}$  at the 15.5 km and below  $6 \times 10^{12}$  molecules  $\text{cm}^{-3}$  at 16 km as measured by the ozonesonde and the lidar correspondingly. Laminated structures were observed in the ozonesonde profiles near the polar vortex edge regions. This together with non-optimal temporal and spatial coincidences between the measurements conducted by different instruments can affect validation accuracy.

### RÉSUMÉ

Le Lidar ozone à méthode d'Absorption Différentielle (DIAL) situé au Polar Environment Atmospheric Research Laboratory (PEARL) à Eureka, Nunavut (80°N, 86°W) s'est avéré être un outil efficace de mesure des profils verticaux d'ozone stratosphérique dans le haut-arctique canadien depuis 1993. Les profils d'ozone mesurés par le lidar lors des campagnes de validation Canadian Arctic Atmospheric Chemistry Experiment (ACE) et Optical Spectrograph and InfraRed Imaging System (OSIRIS) de 2017 ont été comparés aux profils de sondes ozone coïncidentes, ainsi qu'aux profils ozone issus des instruments satellitaires ACE-FTS, ACE-MAESTRO, et OSIRIS. Les résultats de cette validation montrent que le lidar surestime l'ozone d'environ 10% entre 10 et 20 km d'altitude par rapport aux sondes ozone. Au-dessus de 20 km, l'accord entre le lidar et les sondes reste en deçà de 10%. Les données d'OSIRIS et lidar sont en bon accord (10%) entre 15 et 41 km. Durant la phase de validation, une forte baisse d'ozone stratosphérique a été observée le 3 mars 2017, au cours de laquelle la concentration en ozone a diminué jusqu'à  $10^{12}$  molécules  $\text{cm}^{-3}$  à 15,5 km et  $6 \times 10^{12}$  molécules  $\text{cm}^{-3}$  à 16 km, mesurée respectivement par une sonde ozone et le lidar. Des structures stratifiées ont été observées dans les profils de sonde ozone en bordure du vortex polaire. Ces structures, ainsi que les coïncidences temporelles et spatiales non optimales entre les différents instruments, peuvent en partie expliquer l'amplitude des différences observées entre le lidar et les autres techniques.

### ARTICLE HISTORY

Received 30 November 2018  
Accepted 30 July 2019

## Introduction

A large and sudden stratospheric ozone depletion in the Antarctic springtime, as well as a significant decrease of total column content of ozone of the

global scale, was observed at the end of last century (Chubachi and Kajiwara 1986; Farman et al. 1985). Since then, the depletion of the stratospheric ozone layer due to heterogeneous reactions of the ozone-depleting

substances (ODSs) with ozone has been a world-wide concern. The International Vienna Convention of the Protection of the Ozone Layer and the Montreal Protocol and its later amendments were the international agreements to eliminate the production and consumption of ODSs. As a result of implementing the Montreal Protocol the concentration of ODSs in the stratosphere has been declining (WMO 2011). Although many studies have reported that the global ozone is recovering (Jones et al. 2009; Tummon et al. 2015) the WMO assessment 2014 (WMO 2014) has found a slower rate of ozone recovery compared to the previous assessments. While the ozone in the upper stratosphere, between 35 km and 48 km altitude exhibits a significant increase (1.5–2.5% per decade), the ozone in the lower stratosphere (<35 km) has not shown any statistically significant recovery (Steinbrecht et al. 2017). This result has been confirmed by Ball et al. (2018) but challenged by Chipperfield et al. (2018). Based on an additional year of total column satellite observations and 3-D chemical transport model simulations it was shown that the decrease is associated with large inter-annual variability of the ozone due to atmospheric dynamics, which, in turn, emphasizes the need for stratospheric ozone monitoring. Recent findings by Montzka et al. (2018) obtained from the measurements of CFCs and other trace gases in ambient air at several remote sites across the globe for over two decades suggest that one of the main ODSs, CFC-11, has exhibited an increase since 2012 “despite the production being close to zero since 2006” as reported by UNEP (2012). This increase is possibly associated with new production of CFC-11, which is banned by the Montreal Protocol agreement.

Ozone depletion occurs in the Arctic as well. Due to the warmer and shorter winters as well as a less well-developed winter vortex, the ozone depletion in the Arctic is less severe than the Antarctic ozone depletion. However, the Arctic stratosphere is becoming colder (WMO 2011). Recently more severe ozone losses have been observed in the Arctic than have been previously measured; for example, the 2011 Arctic ozone loss (Lindenmaier et al. 2012) was comparable with the Antarctic ozone losses (Manney et al. 2011). Thus, monitoring ozone changes is still necessary and continuing existing long-term measurements is especially valuable.

Satellites and ground-based observations, as well as ozonesonde measurements, have been widely used to measure the concentration of ozone in the atmosphere. Differential Absorption Lidar (DIAL) can be deployed on upward- or downward-looking platforms, has a high temporal and spatial resolution, and it is widely used to measure the vertical distribution. In

the DIAL system two wavelengths are simultaneously transmitted to the atmosphere (Schotland 1964). One wavelength is more absorbed by ozone (the “on-line” wavelength), while the other wavelength is weakly absorbed and used as a reference (the “off-line” wavelength). To retrieve the ozone density profiles, the derivative of the ratio between the number of back-scattered photons as a function of range at two different wavelengths is calculated. The details about the DIAL measurement technique and traditional ozone retrieval algorithm can be found in Schotland (1974), Megie et al. (1977), Godin-Beekmann et al. (2003) and Leblanc et al. (2016a, 2016b) and references therein.

Using a ground-based DIAL system, observations of stratospheric ozone have been performed since 1993 at the Arctic Stratospheric Ozone Observatory in Eureka, Nunavut (80°N, 86°W) (e.g., Steinbrecht 1994; Whiteway and Carswell 1994; Donovan et al. 1995; Pal et al. 1996; Duck et al. 1998; Duck and Whiteway 2005; Kerzenmacher et al. 2005; Dupuy et al. 2009). The DIAL was developed and installed on site by Optech Inc. and the lidar group from York University (Carswell et al. 1991, 1993). Since 2005 the site has been operated by the Canadian Network for the Detection of Atmospheric Change (CANDAC) under the name of the Polar Environment Atmospheric Research Laboratory (PEARL, Fogal et al. 2013). The lidar is a part of the Network for the Detection of Atmospheric Composition Change (NDACC) and has provided the data about ozone distribution in the stratosphere in the Canadian High Arctic for more than 20 years.

In 2009–2015 the Eureka DIAL underwent a major refurbishment and upgrade which brought the system back to full operation in 2017. In this paper the characteristics of the new system are discussed in detail in Section 2. The main objective for the Eureka DIAL is the measurement of stratospheric ozone. Ozone profiles are retrieved using both the elastic and Raman channels of the refurbished system using a traditional ozone retrieval algorithm developed by Leblanc et al. (2016a, 2016b). The example results for a campaign in the spring of 2017, described in Section 3, are available in Section 4. The ozone retrievals were successfully validated against ozonesonde measurements.

## Instrumentation

A schematic of the DIAL is shown in Figure 1. The DIAL consists of transmitter (laser, laser beam steering and shaping optics, Raman cell), receiver

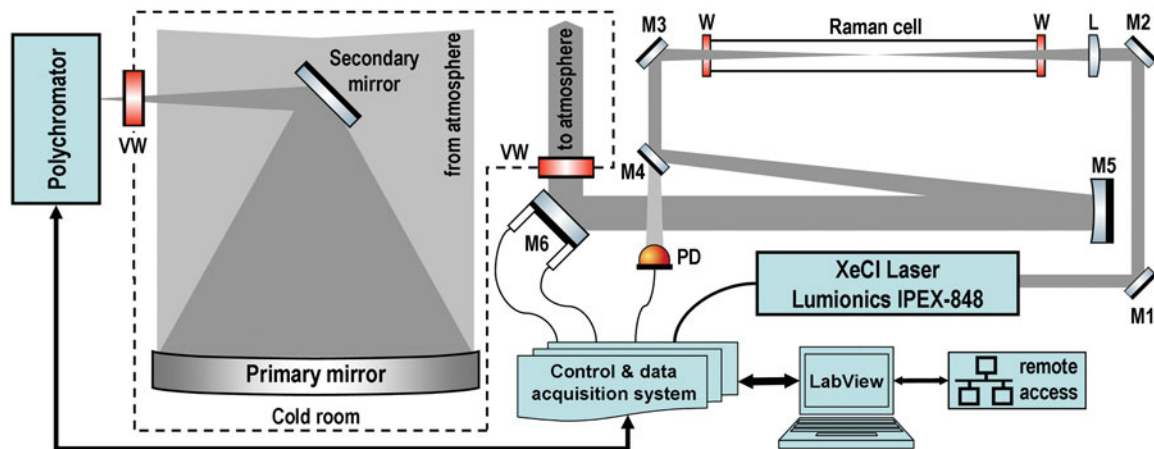


Figure 1. Schematic diagram of the Eureka DIAL system.

(telescope, polychromator) and control and data acquisition system together with a computer. The telescope is kept in a room which opens to the sky by a roof hatch (cold room). This room is physically isolated from the main laboratory which houses the rest of the system and is also optically isolated with an air-lock entry door for entry. The DIAL has five measurement channels. The instrument transmits at 308 and 353 nm. It receives elastic returns at both transmitter wavelengths and inelastic returns at 332, 385 and 405 nm corresponding to Raman scattering of 308, 353 nm light on nitrogen molecules and 353 nm light on water vapour molecules, respectively. The returns are collected in coadd mode at five-minute intervals. The instrument operates during the night time (which at this latitude occurs continuously from late October to late February) and in clear or partiality clear sky conditions. Ratios of the returned profiles can be used for calculations of stratospheric and mesospheric temperature (Carswell et al. 1991, 1993; Steinbrecht 1994; Pal et al. 1996; Donovan et al. 1997; Duck et al. 2000) and tropospheric water vapour (Moss et al. 2012). The system also has been used to study gravity waves (Duck 1999; Duck et al. 2001).

### Transmitter

The two wavelengths transmitted by the lidar are both generated by a single laser, which operates at the ozone DIAL “on line” wavelength of 308 nm. Sending this beam through a hydrogen Raman cell results in 10% of the 308 nm radiation being converted to the ozone DIAL “off line” wavelength of 353 nm. Both wavelengths together then exit the Raman cell and are transmitted to the sky.

The laser’s unstable resonator cavity produces a beam with a divergence of  $400 \mu\text{rad}$ . This low

divergence is critical for efficient Raman conversion to 353 nm. It is also necessary to permit the reduction of the receiver field of view (FOV), thus reducing the level of background radiation entering the receiver.

The original laser was a 308 nm GSI Lumonics Excimer-600 excimer XeCl laser with closed cycle water cooling system. It had a repetition rate of 300 Hz and a pulse energy of up to 200 mJ, giving an average power of up to 60 W. When this laser became inoperable, it was replaced with a new laser with similar specifications. The new laser is a 308 nm IPEX-848 excimer XeCl laser made by LightMachinery Inc. It has a repetition rate up to 200 Hz and a pulse energy of up to 250 mJ, giving an average power of up to 50 W. The characteristics of the new laser are summarized in Table 1.

The beam emerging from the laser is directed by mirrors M1-M2, with an angle of incidence of  $45^\circ$  and a high-reflectance coating that reflects 99% of the light at 308 nm into the Raman cell (Figure 1). The beam passes through a plano-convex lens L with a focal length of 1.4 m. The lens focuses the laser beam at the midway point of the Raman cell. It has an anti-reflection (AR) coating on both sides and transmits 98% of the incident energy at 308 nm. The AR coating maximizes the conversion efficiency of the cell, and limits the damage to the laser windows that might otherwise be caused by excessive laser energy densities if the windows were closer to the focus of the lens. The divergence of the beam going to atmosphere can be optimized. This is done by moving the focusing lens L along the beam.

The Raman cell is a high-pressure gas cell filled with pure hydrogen at 60 psi. It converts a part of the 308 nm laser radiation into radiation at 353 nm through stimulated Raman scattering. The 1st order Stokes output at 353 nm is the reference beam for the

**Table 1.** Characteristics of LightMachinery Inc. IPEX-848 laser.

Specification	LightMachinery Inc. IPEX-848
Laser type	Excimer, XeCl
Wavelength	308 nm
Beam size	10 mm × 22 mm
Divergence	400 $\mu$ rad
Pulse width	<20 ns
Max. repetition rate	200 Hz
Average power	up to 50 W at 200 Hz
Pulse energy	up to 250 mJ

DIAL, because its wavelength is off the peak absorption wavelength for ozone. The Raman cell is a narrow welded aluminum tube 1.8 m long, with an outside diameter of 10.8 cm. At each end of the Raman cell is a high-energy laser window (W) 60 mm in diameter and 10 mm thick. The windows are made of high-quality UV-grade fused silica with broadband (308/353 nm) anti-reflection coatings on both surfaces. The windows have a damage threshold of 20 MW/cm<sup>2</sup>. The cell's input is connected to a hydrogen cylinder via a gas manifold. The cell is also connected at the output end to a vacuum pump to evacuate the gas from the cell. The Raman cell operating parameters have been selected so that it has a conversion efficiency of about 10%. This means that about 10% of the incident laser beam energy is shifted to a wavelength of 353 nm, while 76% of the energy is unshifted and emerges from the Raman cell at 308 nm. The remaining 10% of the energy emerges as higher-order Stokes lines and is not used and 4% is attenuated by the optics. The 1st order Stokes Raman output at 353 nm is also linearly polarized according to the 308 nm input beam. The Raman cell and associated optics are retained from the original lidar (Table 2).

The combined 308 nm and 353 nm beam emerging from the Raman cell is then shaped by beam-collimating optics (Figure 1). The beam is reflected by the plane mirrors M3 and M4 to a spherical mirror, M5, which has a focal length of 4.5 m. Mirror M5 collimates the beam to approximately 150  $\mu$ rad–200  $\mu$ rad and directs the beam onto a mirror, M6, which has an angle of incidence of 45° and is broadband-coated to reflect 99% at 308 and 353 nm. Mirror M6 transmits the beam vertically into the atmosphere through the vacuum window VW between the cold room and the main laboratory. The vacuum window is made of AR-coated fused silica.

Mirror M6 can be adjusted to change the angle at which the output beam propagates into the atmosphere, so that the transmitter beam can be aligned with the receiver FOV. For this reason, the mirror is mounted in a dual-axis gimbal mount equipped with two computer controlled servo actuators that permit

**Table 2.** Specifications of the hydrogen Raman cell.

Parameter	Specification
<b>Input</b>	
Laser wavelength	308 nm
Pulse energy	200 mJ
Pulse duration	<20 ns
Beam divergence	65% of energy within 150–200 $\mu$ rad cone
<b>Optics</b>	
	AR-coated lens (L), $f = 142$ cm
<b>Output</b>	
Fundamental component (308 nm)	152 mJ
1st Stokes component (353 nm)	20 mJ
Losses in higher Stokes components	20 mJ
Losses in optics	8 mJ (4%)
FWHM (308 and 353 nm)	0.3 nm
<b>Physical dimensions</b>	
Length	1.8 m
Clear aperture diameter	50 mm
Optical windows (W)	10 mm thick, AR-coated
Maximum rated pressure	300 psi
Operating pressure	60 psi

an adjustment of the laser beam in North-South and West-East directions with a resolution of 4  $\mu$ rad. Once the return signals in 308 nm and 353 nm channels at 10 km range are maximized by these adjustments, the transmitter beam is considered to be aligned within the receiver FOV and the full overlap between the transmitter beam and the receiver FOV is maintained. Specification of the mirror gimbal mount is summarized in Table 3.

### Receiver

The receiver consists of a telescope and polychromator. The telescope is an  $f/2.5$  Newtonian with a 1 m diameter primary mirror (2.5 m focal length) mounted on an 18-point flotation system. The mirror is coated with aluminum and a protective over-coating of SiO<sub>2</sub>, providing a reflectivity of better than 90% in the UV region. Like the primary mirror, the secondary mirror is coated with aluminum and a protective over-coating of SiO<sub>2</sub>. It is mounted at a 45° angle and reflects better than 90% of the backscattered radiation into the polychromator (Figure 2) at an angle of 90° to the telescope axis.

The polychromator implements the following functions: separating the wavelengths, distributing each wavelength to the designated PMT for signal detection and photon counting, and background signal reduction. Before the received light enters the polychromator it passes through another vacuum window VW (Figure 1) similar to one in the transmitter part of the DIAL. In the polychromator the radiation is split into 308, 332, 353, 385 and 405 nm wavelengths, filtered by the secondary optics, and directed to separate PMTs. The 308/353 nm wavelength pair serves for elastic “on line/off line” ozone detection, 332/385 nm - for

Raman “on line/off line” ozone detection, and 405/385 nm - for Raman “on line/off line” water vapour detection. The optical chopper (OC) blocks backscattered light from low altitude in the 308 and 353 nm channels that would otherwise be too intense for photon counting.

Two filter wheels with neutral density filters (NDF) in the 308 and 353 nm channels provide the capability to control the intensity of the radiation entering PMT detectors and prevent their saturation. Each filter wheel contains five neutral density filters with optical densities of 0, 0.5, 1, 2, and 3. The wheel is motorized and under computer control. The choice of filter

**Table 3.** Specifications for the M6 collimating mirror gimbal mount.

Parameter	Specification
Gimbal mount	
Model	Newport SL 15
Optics diameter	6.0" (152.4 mm)
Adjustments	$\Theta_x, \Theta_y$
Sensitivity	4 $\mu$ rad
Angular range	$\pm 1.15^\circ$
Servo actuators	
Model	Newport CONEX-TRA25CC
Travel range	25 mm
Minimal incremental motion	0.2 $\mu$ m
Control interface	USB

depends on the intensity of the incoming radiation. Radiation in each channel is then spectrally filtered at the appropriate wavelength by a 25 mm diameter narrow bandpass interference filter (IF). The specification of the receiver is summarized in Table 4.

The OC in the 308 nm and 353 nm channels provides gating of the receiver FOV, so that the low-altitude return signals in the elastic channels that would be too intense for the detection system are physically blocked. The OC also acts as the system’s master trigger. The current OC has a four slot blade and a brushless DC motor. Its rotation speed is set to 8,910 rpm. The OC output signal frequency is 594 Hz but the trigger pulse is produced on every third slot to trigger the laser at 198 Hz. The OC is controlled by a proportional–integral–derivative (PID) controller based on an ATmega328 micro-controller. OC specifications are summarized in Table 5. The time it takes for the OC to open the receiver FOV depends on the size of the focal spot in this plane. To minimize the collection of ambient light, the receiver FOV is kept small. The field stop (FS) sub-assembly consists of a motorized adjustable iris under computer control.

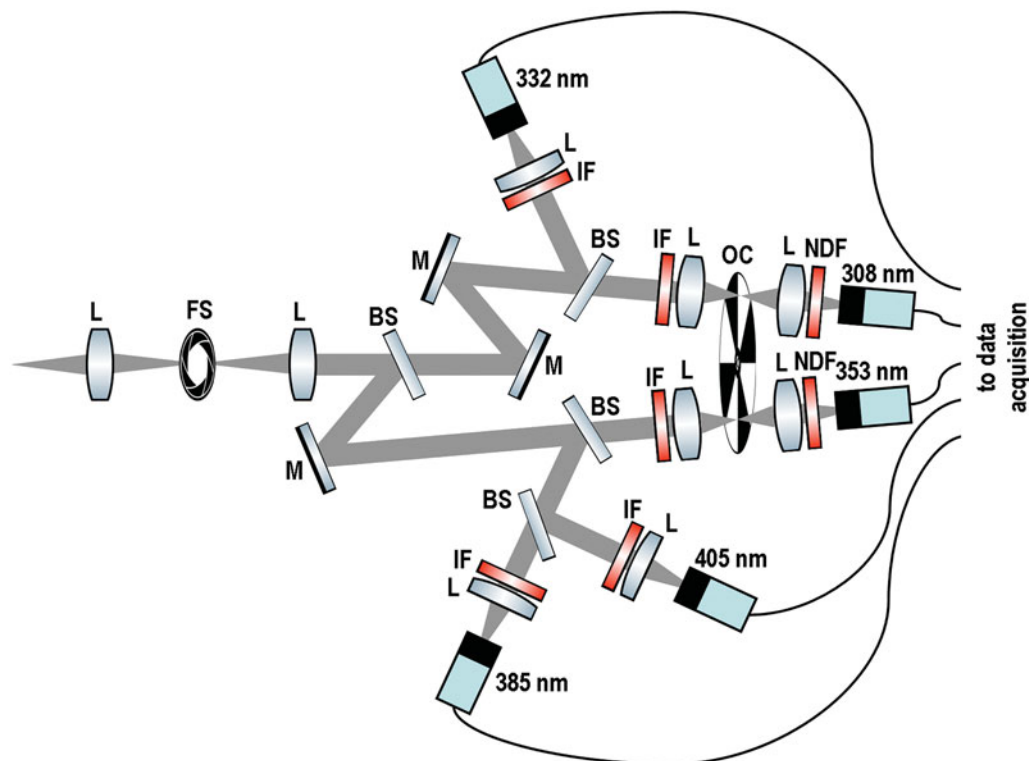


**Figure 2.** Schematic of the polychromator. Light from the telescope is focused through the field stop (FS), collimated, and split between elastic and Raman channels by a set of mirrors (M) and beam splitters (BS). Other components include lenses (L), interference filters (IF), neutral density filters (NDF), the optical chopper (OC) and the photomultiplier tubes (indicated by wavelength).

**Table 4.** DIAL receiver specifications.

Parameter	Specification		
Telescope type	1 m diameter Newtonian, $f = 2.5$ m, Al + SiO coated		
Aperture FOV	0.2–1 $\mu$ rad		
Neutral density filters	Notation	OD	T(%)
	ND0	0	100
	ND0.5	0.5	31.6
	ND1	1	10
	ND2	2	1
	ND3	3	0.1
Interference filters	Central wavelength	T(%)	FWHM (nm)
	308 nm	>40	20
	331.9 nm	>50	2
	353 nm	>50	2
	385 nm	>50	0.5
	405.3 nm	>60	10

**Table 5.** Specifications of the optical chopper.

Parameter	Specification
Blade	4-slot
Motor	Brushless DC (Koford Engineering., LLC)
Speed	8910 rpm
Laser triggering	198 Hz (every 3rd slot)
Control	PID

### Signal-processing hardware

The signal-processing hardware consisting of amplifiers, discriminators and counter boards, is a part of the control and data acquisition system. The amplifiers, Quad DC-300 MHz Phillips Model 770, amplify the voltage output from the 308, 332, 353, and 385 nm PMTs (Thorn EMI 9893/350). The discriminators, Quad 300 MHz Phillips Model 704, accept pulses from the amplifiers and discard those with an amplitude below a preset threshold. They then convert pulses above the threshold into pulses with a constant duration and amplitude. The signals from the discriminators pass to two dual-channel counter boards for pulse counting. The 405 nm channel uses a PAD-1G unit made by Optech Inc., which holds PMT, amplifier and discriminator in one housing. Three ISA bus-based dual-channel counter boards, Optech Inc. FDC-700M, are used in the DIAL. DIAL optical detectors and signal-processing hardware specifications are summarized in Table 6.

During the upgrade a custom ISA-to-USB adapter was designed and built to interface the counter boards with a modern PC. The adapter consists of an Altera Cyclone IV Field Programmable Gate Array (FPGA) Development Board simulating the necessary aspects of the ISA bus operation, integrated with a Future Technology Devices International Limited (FTDI) FT2232H USB 2.0 UART/FIFO mini module, used as an interface between PC and FPGA. The code for the FPGA is written in Verilog Hardware Development Language using Altera Quartus II programmable logic device design software.

**Table 6.** DIAL optical detectors and signal-processing hardware specifications.

Specification	Channel				
	308 nm	332 nm	353 nm	385 nm	405 nm
PMT	Thorn EMI 9893/350			Hamamatsu H5783P-03	
Amplifier	Phillips 770			Optech Inc. PAD-1G	
Discriminator	Phillips 704			Optech Inc. PAD-1G	
Counter board	Optech Inc. FDC-700M, 2 ch, 8 bit/ch, 700 MHz				

### Control and operation

The DIAL is controlled by custom software written in LabView. The software has a user-friendly interface and allows the control of every subsystem of the DIAL, provides the capability to measure in manual or scheduler mode, and displays raw data in real time. Additionally the upgrade of the DIAL system opened the possibility to operate the instrument remotely which has not been an option before.

The PEARL RidgeLab, housing the DIAL, is 15 km away by road from the Eureka Weather Station, which provides accommodation for lidar operators. In the past, there were nights which were appropriate for DIAL measurements, but which were not appropriate (due to weather and other safety and logistical factors) for travel between the sites. In those cases, the DIAL did not make measurements. Since the DIAL refurbishment, the operator can initiate, monitor, and terminate DIAL operations remotely from the Weather Station, resulting in more measurement periods of longer duration. Laser optics cleaning and gas refilling are still carried out on-site in the laboratory.

### 2017 Canadian Arctic Atmospheric Chemistry Experiment and Optical Spectrograph and InfraRed Imaging System Validation Campaign

The measurements with the newly refurbished DIAL were carried out in Eureka during the 2017 Canadian Arctic Atmospheric Chemistry Experiment (ACE) and Optical Spectrograph and InfraRed Imaging System (OSIRIS) Validation Campaign. These campaigns have been conducted annually since 2004 to provide correlative data for validating measurements from the ACE satellite mission, launched by Canadian Space Agency onboard the SciSat in August 2003 (Bernath et al. 2005) and Canada's OSIRIS instrument, launched onboard Swedish satellite Odin in February 2001 (Llewellyn et al. 2004). During these campaigns (see for example Kerzenmacher et al. (2005), Adams et al. (2012), Griffin et al. (2017) and references therein) a set of ground-based instruments have been deployed at PEARL to measure trace gases in the

Arctic atmosphere during the polar sunrise period from the end of February to early April.

There are more than a dozen instruments typically deployed during the campaign and at least half of them measure ozone. Other than the DIAL, most of the ground-based ozone-sensitive measurements are made by sun-viewing column-measuring instruments, which are restricted to daytime operations. Except of the ozonesonde, the DIAL is the only campaign instrument with true vertical ozone profiling capability, since it detects the backscattered returns versus the range.

The DIAL began to operate during the 2017 pre-campaign phase, from January 25 to February 25, 2017. DIAL measurements then continued during hours of darkness through the intensive-campaign phase, which ran from February 26 to March 13, 2017. DIAL measurements ended on March 10, when the duration of the night between nautical dusk and nautical dawn fell below 5 hours. The daytime campaign instruments began measurements on February 25, after polar sunrise, and continued during the extended phase of the campaign until April 2017.

### **Eureka Weather Station ozonesondes and radiosondes**

Lidar-sonde comparisons are a common approach for validation. The Eureka Weather Station launched Vaisala RS92 radiosondes routinely twice a day at 11:15 and 23:15 UTC during the year. Radiosondes provide vertical profiles of pressure, temperature, relative humidity, wind speed and direction from the ground up to 30 km–35 km with vertical resolution less than 50 m. The station also launches electrochemical concentration cell ozonesondes (ECC, EN-SCI, Model Z) typically once per week through the year (Tarasick et al. 2005), with the frequency of the sondes increased during the campaign up to one per day, weather permitting. The ozonesondes are launched on Raven brand high-strength polyethylene balloons when possible. These balloons provide smaller rates of ascent and can reach higher altitude in comparison with Totex brand latex balloons, which can be launched during windier conditions than is allowable for the Raven balloons. Typical vertical resolution of the ozonesondes is 100 m–200 m. The ozonesonde preparation procedures followed Davies et al. (2007) and Tarasick et al. (2005): 2.5 mL of 1% buffered potassium iodide solution was used in the cathode chamber and a pressure-dependent background correction was applied.

The ozonesonde measurements provide an independent validation for the DIAL ozone measurements. They are not strictly co-located measurements, since they are launched 12 km away from the lidar. The sonde drifts toward and/or away from lidar as it rises, depending upon wind direction and because of that the ozonesonde and the DIAL may sense different air masses on a given night. However, ozonesondes still provide high-resolution *in-situ* vertical profiling information, which is a valuable comparable.

### **Satellite ozone measurements**

The ACE mission includes two instruments: a high spectral resolution infrared Fourier Transform Spectrometer (ACE-FTS) and the Measurement of Aerosol Extinction in the Stratosphere and Troposphere Retrieved by Occultation instrument (ACE-MAESTRO). ACE-FTS has a resolution of  $0.02\text{ cm}^{-1}$  and operates from  $750\text{ cm}^{-1}$  to  $4,400\text{ cm}^{-1}$  (Bernath et al. 2005). ACE-MAESTRO is a dual UV-visible-near-infrared spectrometer measuring in the spectral regions between 285 nm and 1015 nm (McElroy et al. 2007). Both the ACE-FTS and ACE-MAESTRO make measurements in the solar occultation mode and examine almost the same slant column of air. The ACE mission is designed to measure atmospheric spectra to obtain vertical distribution of gas species, aerosol, temperature and pressure from the ground up to 100 km. It is focused on investigation of chemical and dynamical processes in the atmosphere with a particular emphasis on trace gases in the Arctic atmosphere. ACE-FTS Level 2 data product (current version 3.5/3.6) provides vertical profiles of several gas species including ozone with vertical resolution of  $\sim 4\text{ km}$ . ACE-MAESTRO Level 2 data product (current version 3.13) provides vertical profiles of ozone, aerosol extinction and total optical depth with vertical resolution of 1–2 km. The OSIRIS instrument is a grating optical spectrograph that measures spectra of limb scattered sunlight from the upper troposphere into the lower mesosphere within 280 nm–800 nm spectral range (Llewellyn et al. 2004). The measurements are used to produce vertical profiles of  $\text{O}_3$ ,  $\text{NO}_2$ , and stratospheric aerosols. OSIRIS Level 2 data product (current version 5.10) provides the ozone number density vertical profiles over the altitude range from 10 km to 60 km at a vertical resolution of 2–3 km.

### **DIAL setup and processing methods**

During the campaign the DIAL was set up to perform measurements in four step intervals. Each interval lasted for 5 minutes during which elastic and Raman



backscattered signals from 59400 laser shots were collected, summed together and saved. During the first step (elastic-low) the OC for the elastic channels (308 and 353 nm) was set to cut off signals below 3 km and ND3 filters were placed in front of the PMTs to prevent any saturation from high-intensity backscatter returns from low altitudes. During the second step (elastic-middle) the OC cutoff altitude was 7 km and the measurements were done with ND2 filters in the elastic channels. Steps three and four (elastic-high) were identical to each other with a 15 km OC cutoff altitude and no neutral density filters in front of the PMTs. Due to the much smaller Raman returns at 332 and 385 nm it is not necessary to attenuate these signals using neutral density filters or to block the low altitude returns with OC, so during all four steps the Raman channels measure backscatter returns from the entire vertical column of the atmosphere and the settings of the Raman channels remain unchanged. In both elastic and Raman channels the backscatter returns are collected in the range from the ground up to 150 km with a resolution (single bin size) of 150 m.

A traditional data-processing algorithm is used to retrieve ozone vertical profiles from DIAL backscattered signals. During the data processing the ozone number density profiles calculated from elastic and Raman channels are merged together and averaged in time to generate either a nightly mean ozone profile, or a mean profile over some other predetermined time interval. With lidar data processing we follow the guidelines of the NDACC Lidar Working Group described in detail by Leblanc et al. (2016a, 2016b).

## Results

An example of the nightly mean DIAL ozone vertical profiles retrieved for each step of the DIAL operation sequence during the night on January 25, 2017 is shown in Figure 3. As can be seen from the figure all elastic and Raman profiles are close to each other. The elastic-low profile provides minimal statistical uncertainty of 2–3% up to 17 km altitude region, while its vertical resolution varies between 1.6 km and 3 km. Raman and elastic-middle profiles provides similar 2–3% value of uncertainty up to 22 km altitude region, while their vertical resolution is  $\sim 0.8$  km below 15 km altitude and increases up to 3 km in the altitude range between 15 and 22 km. The optimal measurements for the altitudes above 17 km are provided by elastic-high profiles with maximum uncertainty of 3% up to 35 km and increasing up 40% above 35 km altitude. To obtain resultant DIAL ozone

vertical profiles, Raman and elastic profiles are merged together such that optimal values of uncertainty and vertical resolution are retained.

DIAL ozone profiles have been compared to the data from ozonesondes, ACE-FTS, ACE-MAESTRO and OSIRIS. There were 31 observational DIAL nights in total and 9 ozonesondes were launched from the Eureka Weather Station for the period of the campaign. The coincidence criteria for comparisons between DIAL and ozonesonde were taken to be a maximum of 12 hours time difference between the average time of the DIAL measurement and the mid-way time point between launch and burst of the ozonesonde. The sonde launched on January 25, did not satisfy coincidence criteria and two sondes, launched on February 15 and March 9, failed to reach 10 km altitude. Those three cases have been excluded from the analysis making six coincidences in total when DIAL measurements match the ozonesonde launches, i.e., on February 9 and 24, March 1, 2, 3 and 5. To compare DIAL ozone profiles to the satellite data the ozone profiles from ACE occultations and OSIRIS limb measurements that occurred within 200 km radius from the PEARL Ridgelab during the DIAL operation period were considered. A temporal coincidence criteria similar to one applied to the DIAL-ozonesonde comparisons ( $\pm 12$  hours difference between the measurements) was used to compare DIAL results to ACE-FTS, ACE-MAESTRO and OSIRIS data. The ACE occultation on February 24 did not satisfy  $\pm 12$  hours coincidence criteria while the ACE-MAESTRO profile on February 26 had anomalously large uncertainties, which resulted in four ACE-FTS (on February 25, 26, 27 and 28) and three ACE-MAESTRO (on February 25, 27 and 28) ozone profiles taken for comparison to DIAL ones. OSIRIS had four limb measurements on February 28 and March 2, 4 and 5. All four of them satisfied  $\pm 12$  hours coincidence criteria. Figure 4 shows DIAL nightly mean profiles compared to the coincident ozonesonde, ACE-FTS, ACE-MAESTRO and OSIRIS profiles. Shadings in subplots represent the uncertainties: total combined uncertainty for the DIAL as per the definition from Leblanc et al. (2016b), which is kept at  $\sim 3\%$ , and 10% uncertainty for the ozonesondes. Also thick blue dashed curves on the subplots depict vertical resolution of the DIAL retrieval. Error bars in the subplots represent statistical error of ozone retrieval for ACE-FTS, a random error due to instrument noise propagated through the spectral fitting and vertical profile retrieval code for ACE-MAESTRO and standard uncertainty of ozone concentration for OSIRIS

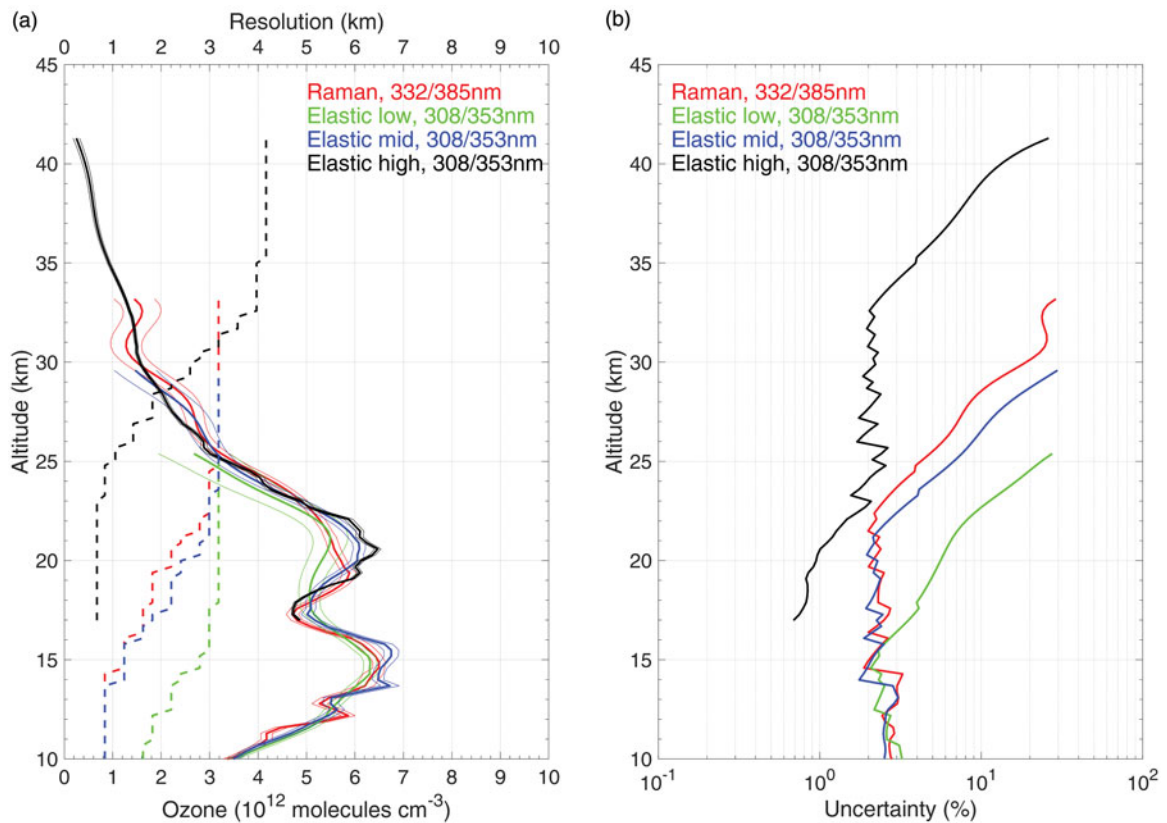


**Figure 3.** Example of elastic and Raman ozone DIAL profiles obtained on January 25, 2018. Vertical resolution for each measurement step (Raman, elastic-low, elastic-middle, elastic-high) is shown in dashed lines in subplot (a). Statistical uncertainty for each measurement step is shown in thin solid lines in subplot (a) and in thick solid lines in subplot (b).

profiles. The DIAL profiles demonstrate the refurbished DIAL's basic competence in producing ozone profiles that match the output of the associated ozonesondes and satellite instruments in most of the cases.

To verify the conditions of the measurements of the ozone vertical profiles, total ozone column obtained from Brewer spectrometer (Fioletov et al. 2005) and University of Toronto Ground-Based Spectrometer (UT-GBS, Fraser et al. (2008)) co-located with the DIAL as well as scaled potential vorticity (sPV) calculated based on Modern Era Retrospective-analysis for Research and Applications data products (NASA 2019) were considered (Figure 5). MERRA2 sPV is a parameter used to estimate the location of the polar vortex edge. Although Ertel's potential vorticity (PV) is the natural variable to study in and out vortex changes at a specific potential temperature level, sPV, i.e., PV divided by a standard value of static stability, is better suited for studying the vertical structure of the vortex edge. Details on sPV calculations can be found in Dunkerton and Delisi (1986) and Manney et al. (1994).

DIAL, ozonesonde, ACE-FTS, ACE-MAESTRO and OSIRIS profiles averaged over the particular

coincident nights during the campaign are shown in Figures 6–10. To obtain the average profiles, the coincident profiles were interpolated on a 0.2 km altitude grid and the arithmetic mean was calculated. Dashed lines in Figures 6–10 (a) represent the uncertainties that were calculated in the following way (Leblanc et al. 2016b; JCGM 2008a, 2008b, 2009, 2012). For each altitude point in the DIAL profile, the root sum square of the random uncertainties of coincident nightly mean profiles was taken and averaged. Then for each altitude point the arithmetic average of the systematic uncertainty of coincident nightly mean profiles was taken. The mean DIAL uncertainty (blue thin solid line in Figures 6–10, subplot (a)) was calculated by taking a root sum square of the averaged random and systematic DIAL uncertainties. For the ozonesonde for each altitude point the root sum square of 10% uncertainty of coincident profiles was taken and averaged (black thin dashed line in Figures 6–10, subplot (a)). The uncertainties for ACE-FTS, ACE-MAESTRO and OSIRIS were estimated in a similar way as for the ozonesonde taking into account the definitions of the measurement errors and uncertainties for each satellite instrument. Finally the root

sum square of DIAL, ozonesonde, ACE-FTS, ACE-MAESTRO and OSIRIS uncertainties were taken to estimate the uncertainty of the difference (black thin dashed lines in Figures 6–10, subplots (b) and (c)).

## Discussion

Figure 4 shows nightly mean DIAL together with coincident ozonesonde, ACE-FTS, ACE-MAESTRO and OSIRIS ozone profiles. In general the DIAL ozone

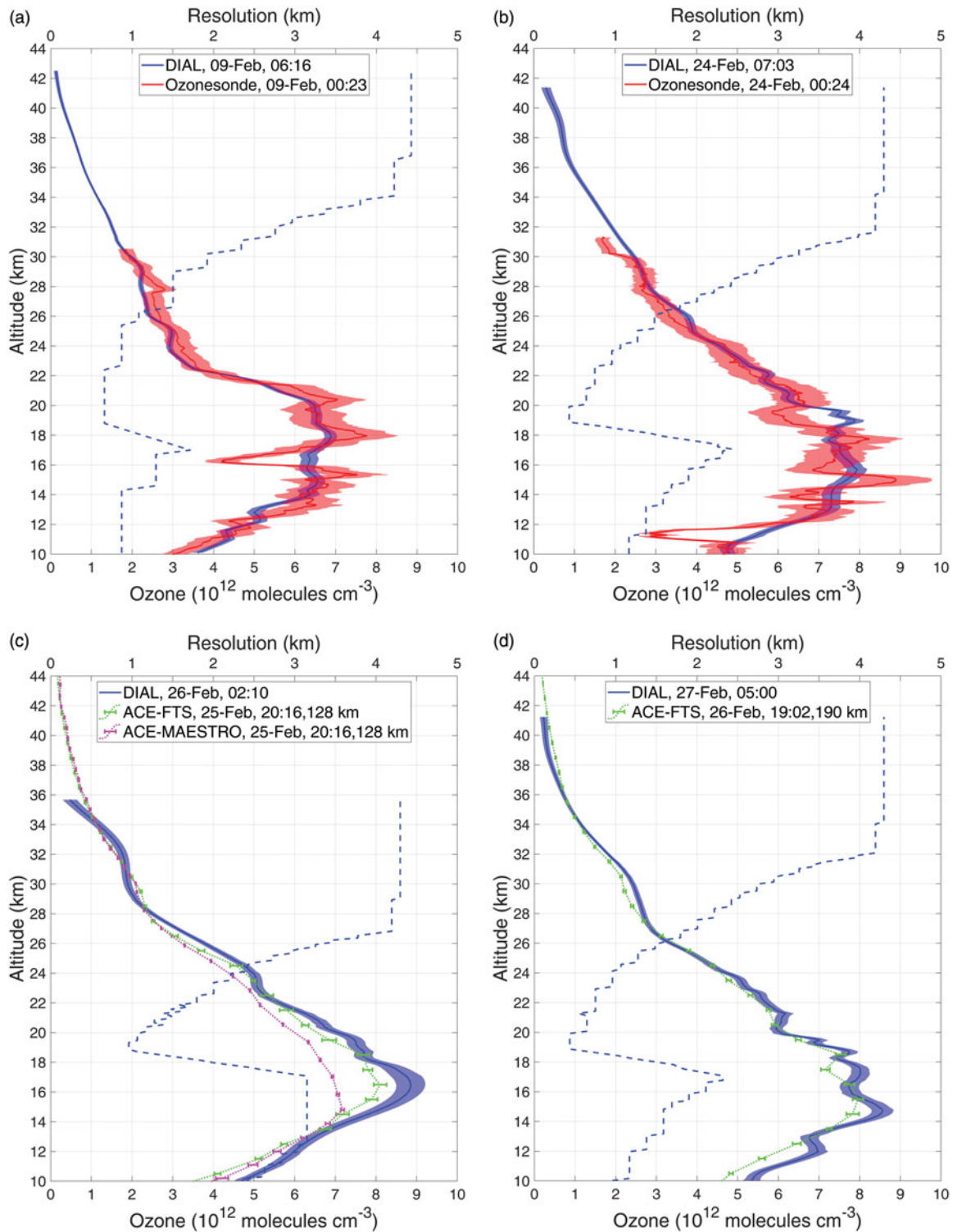


**Figure 4.** Coincident ozone profiles measured by the DIAL, ozonesonde, ACE-FTS, ACE-MAESTRO and OSIRIS. The shading denotes total combined uncertainty for the DIAL and 10% uncertainty for the ozonesondes. Blue thick dashed curve depicts vertical resolution of the DIAL. Error bars represent statistical error of ozone retrieval for ACE-FTS, a random error due to instrument noise propagated through the spectral fitting and vertical profile retrieval code for ACE-MAESTRO and standard uncertainty of ozone concentration for OSIRIS profiles.

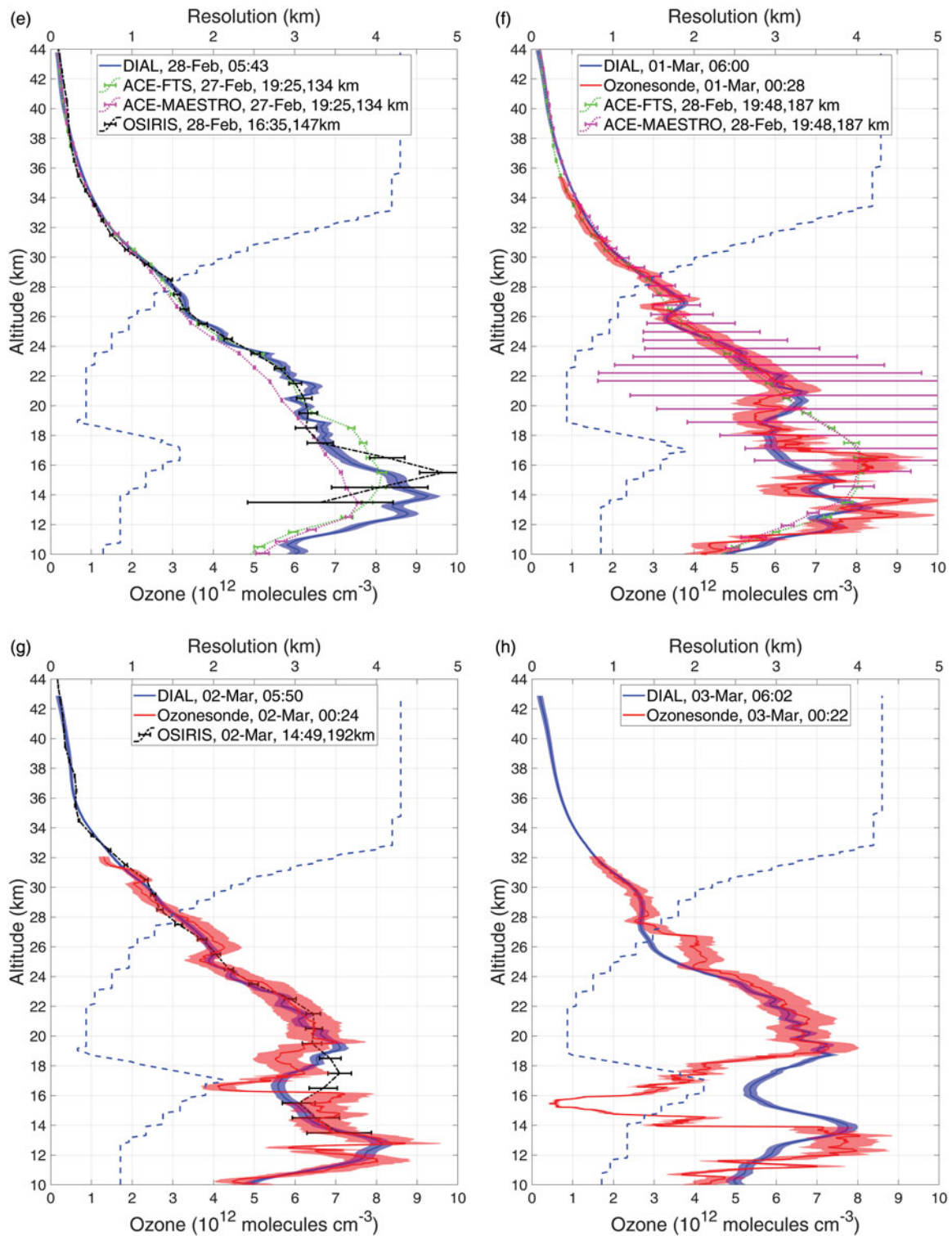


Figure 4. (Continued).

retrievals are a close match to the ozonesondes, with exception of several narrow features observed at various altitudes in the ozonesonde profiles due to their finer vertical resolution, typically about 200 m or better. For example, those are visible on February 9, 24 and March 1, 2 (Figure 4 (a), (b), (f) and (g)). These

features represent sharply defined layers of higher or lower ozone concentration called positive and negative laminae, correspondingly. More details on ozone laminae and their physics can be found in Bird et al. (1997) and Krizan et al. (2015) and references therein. According to the studies such filamentous layers in

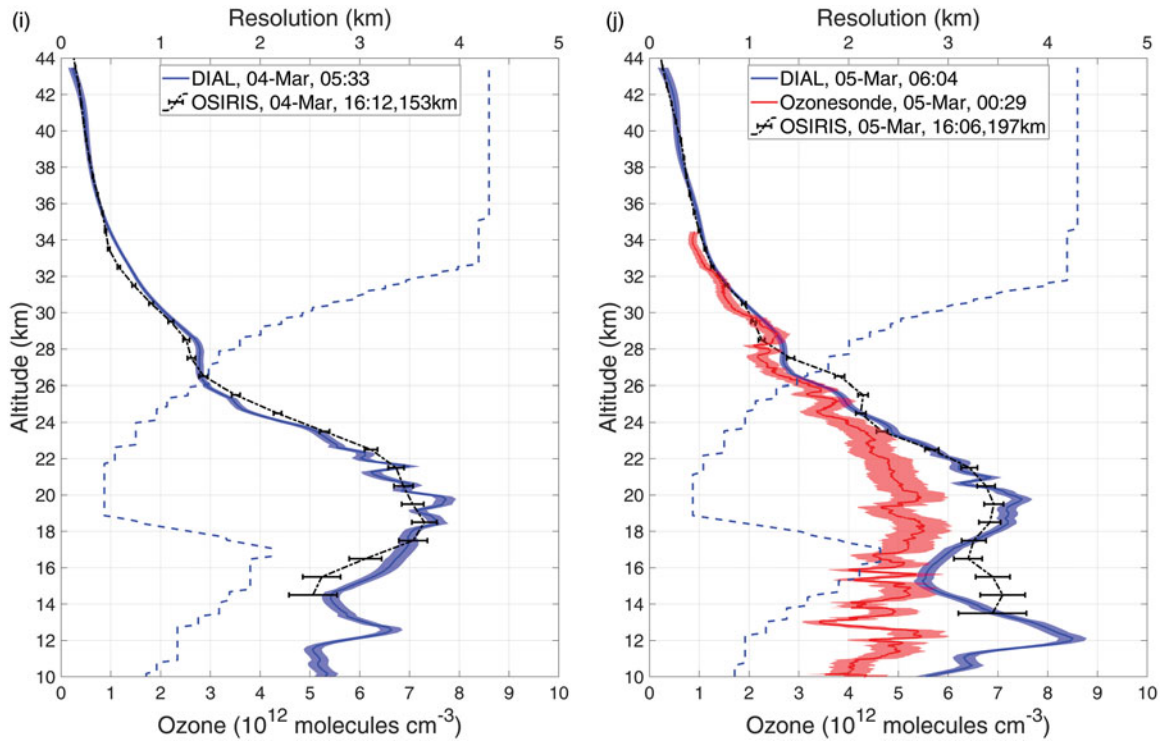


Figure 4. (Continued).

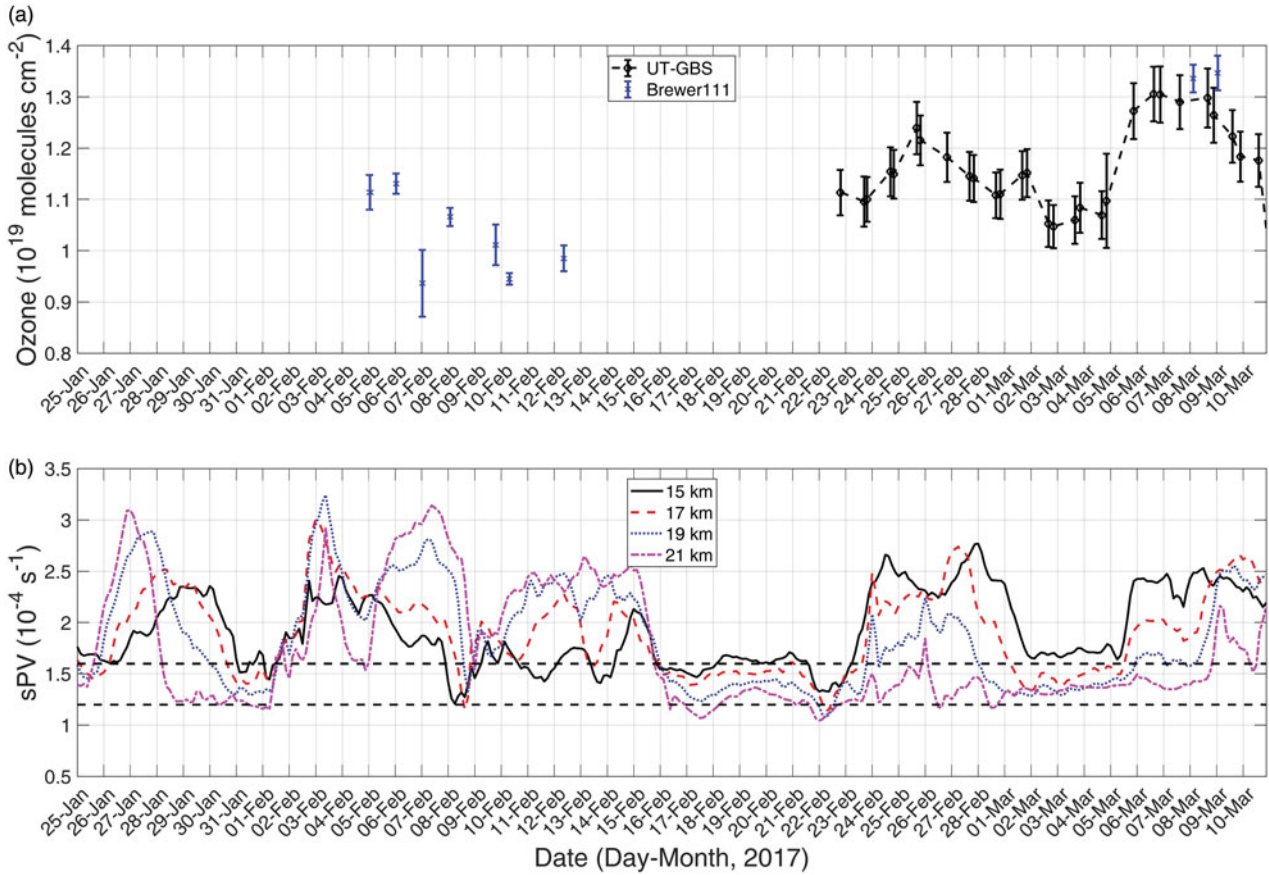
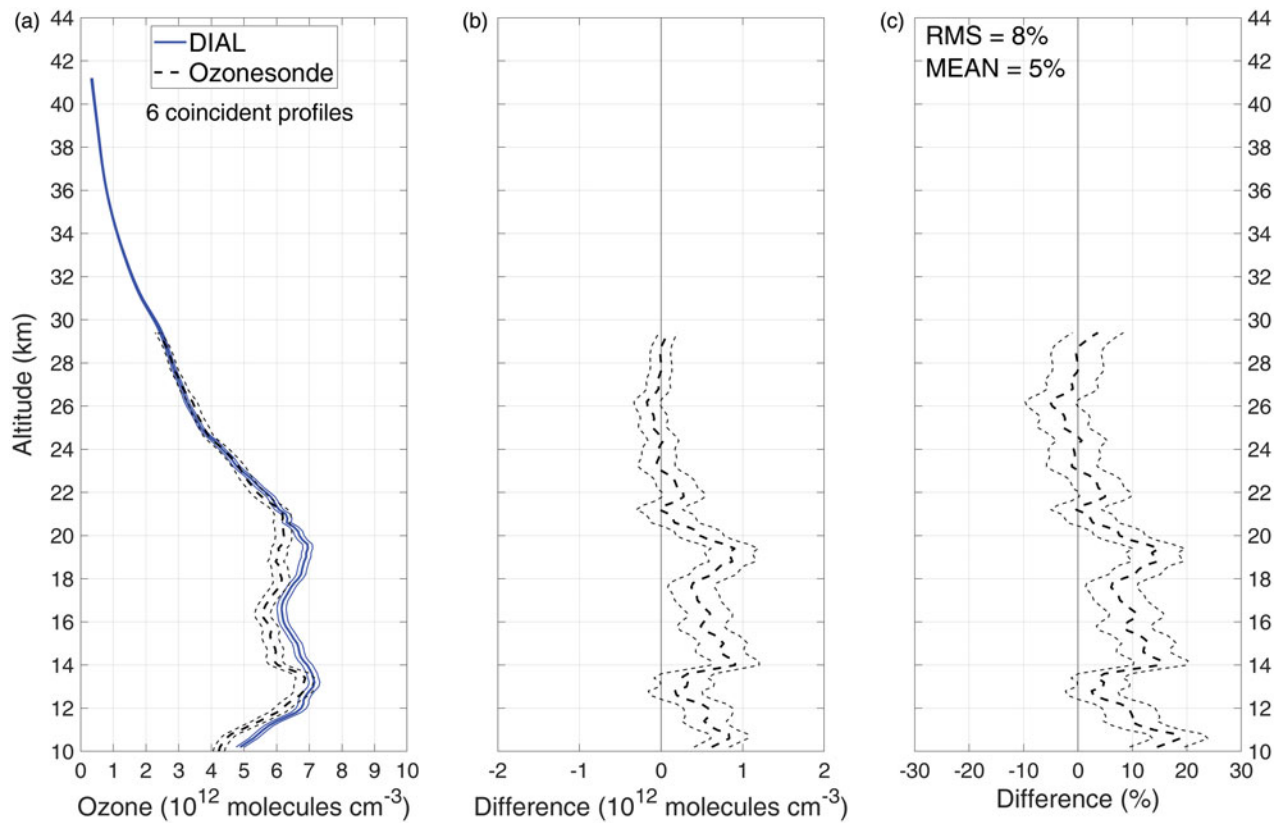


Figure 5. Time series showing ozone total column from Brewer and UT-GBS (a) and MERRA2 sPV at 15 km–21 km levels (b) during the period between January 25 and March 11, 2017. The approximate values of sPV corresponding to the position of inner and outer edges of the polar vortex are marked by dashed lines.



**Figure 6.** Mean ozone profiles and differences measured by DIAL and ozonesonde, including all six coincident cases. (a) ozone number density. (b) absolute difference (DIAL - ozonesonde). (c) the difference relative to the ozonesonde in percent:  $100 \times (\text{DIAL} - \text{ozonesonde})/\text{ozonesonde}$ . Dashed lines in subplot (a) for the DIAL represent random and systematic uncertainties summed in quadrature; for the ozonesonde - 10% uncertainty for each profile summed in quadrature. Dashed lines in subplots (b) and (c) depict the resultant uncertainty which is DIAL and ozonesonde uncertainties summed in quadrature (see details in text).

the ozone vertical profiles most frequently occur in lower stratosphere around 14 km altitudes at the polar vortex edge. The laminae are difficult to resolve by lidar or satellite instruments due to their poorer vertical resolution and therefore this can affect the satellite-ozonesonde or lidar-ozonesonde validation accuracy. For example, the resolution of Eureka DIAL ozone retrievals varies in the range between 300 m and 5 km (see blue thick dashed curves in Figure 4). Also the duration of the ozonesonde flight is between 1.5 to 2 hours depending on the type of balloon used and burst altitude, while the ozone profile from the DIAL is the result of the measurements averaged over the entire night.

Reasonable agreement can be observed between DIAL ozone profiles and the profiles obtained from both ACE mission instruments. Some disagreement is seen on February 26 when DIAL overestimates the ozone by as much as 10% below 17 km and by 15–20% below 22 km altitudes in comparison with ACE-FTS and ACE-MAESTRO respectively (Figure 4 (c)). On March 1, 2017 (Figure 4 (f)) a beginning of ozone depletion event was captured by DIAL and ozonesonde around 19 km. In fact, ACE-

FTS and ACE-MAESTRO overestimated ozone by up to 25–30% around 19 km in comparison with DIAL on that date. The depletion persisted on March 2 (Figure 4 (g)) as measured by the DIAL, ozonesonde and OSIRIS. All three instruments showed reasonable agreement between each other. The ozone reached its minimum on March 3 with a drop in the ozone number density of  $\sim 1 \times 10^{12}$  molecules  $\text{cm}^{-3}$  around 15.5 km according to the ozonesonde (Figure 4 (h)). During the flight the ozonesonde drifted  $\sim 100$  km southward from Eureka. The DIAL did provide a similar vertical pattern as the ozonesonde, but the minimum value of ozone in the DIAL measurement was significantly larger than in the ozonesonde measurement. On March 4 (Figure 4 (i)) the stratospheric ozone around 16 km recovered, reaching the level of  $6.5 \times 10^{12}$  molecules  $\text{cm}^{-3}$  according to both DIAL and OSIRIS, while the ozone around 12 km–14 km experienced a drop in comparison with the previous night. Both instruments DIAL and OSIRIS showed good agreement between each other. On March 5 (Figure 4 (j)) the ozone around 15 km experienced another depletion with ozone concentration close to

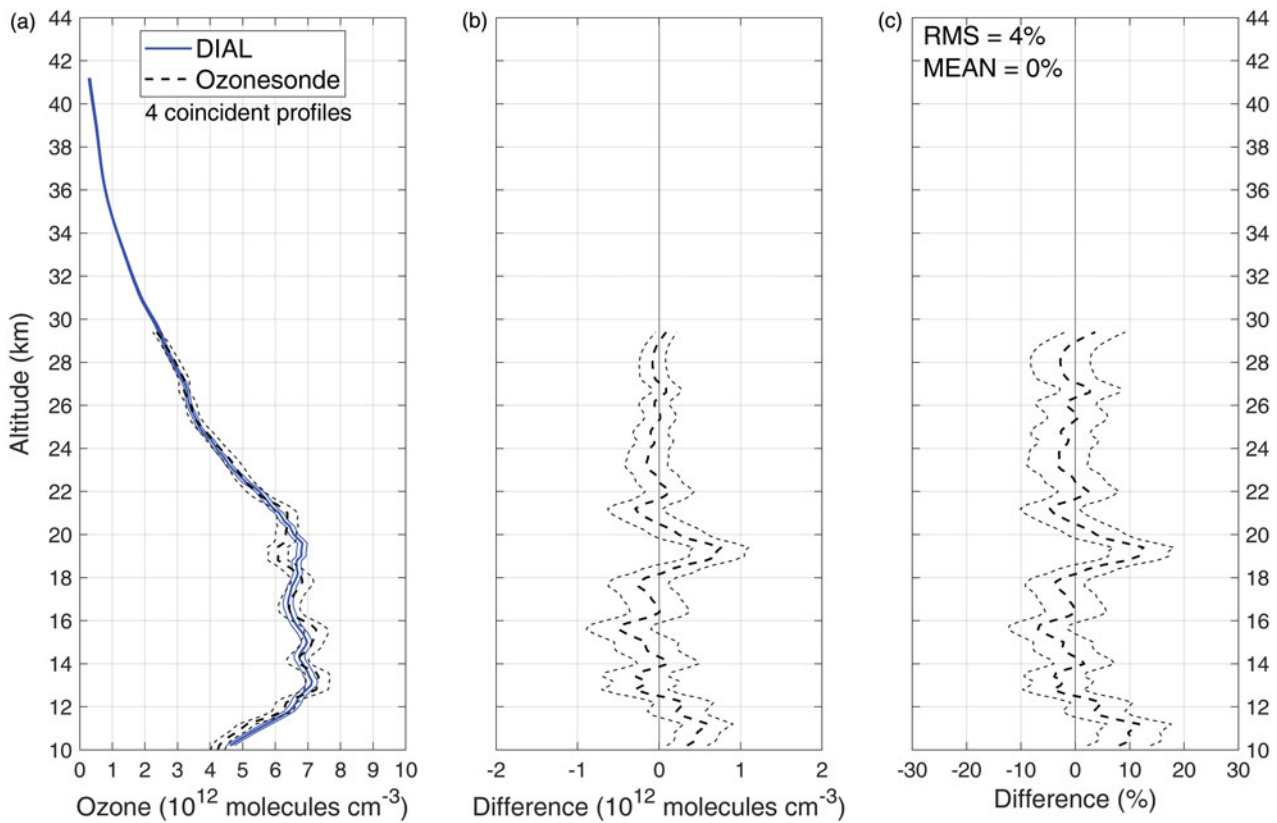


**Figure 7.** Mean ozone profiles and differences measured by DIAL and ozonesonde, excluding coincident cases on March 3 and 5.

$5.5 \times 10^{12}$  molecules  $\text{cm}^{-3}$  as measured by the DIAL. However, the ozone around 12 km region exhibited a 30–40% increase in comparison with the results from March 4. In contrast, the ozonesonde profile for March 5 showed ozone depletion with concentrations close to  $5 \times 10^{12}$  molecules  $\text{cm}^{-3}$  along the entire altitude range between 10 and 24 km. During the flight the ozonesonde drifted  $\sim 90$  km from Eureka in south-west direction. Overall for March 5 the DIAL ozone values are more than 50% larger than those for the ozonesonde around 18–20 and 12 km regions. A 20–25% ozone underestimation is observed in DIAL profile in comparison with OSIRIS profile at 15 km altitude region, while above 18 km the DIAL and OSIRIS profiles have good agreement between each other. Unfortunately, there were neither satellite measurements on March 3 nor ozonesonde launches on March 4 coincident with DIAL that could provide better understanding of the situation.

According to the data from Brewer and UT-GBS, total ozone column exhibits a decrease between March 1 and 3 and then increases rapidly between March 5 and 6 (Figure 5 (a)). Analysis of total ozone maps provided by the Environment and Climate Change Canada (ECCC) and available at the World Ozone and Ultraviolet Radiation Data Centre

(WOUDC 2019) indicates that between March 3 and 10 Eureka was on the edge of a large region of high total ozone column values with a strong spatial gradient of ozone towards the south-west direction. The observed values of the ozone total column correlate well with MERRA2 sPV values for four altitudes in lower stratosphere: 15, 17, 19, and 21 km shown in Figure 5 (b). According to PV maps (GEOS-5.12.4, 2019, JPL) the vortex edges were well defined during the DIAL operation period, however the location of the vortex was unstable in relation to Eureka. Quite often the edge of the vortex was located in the vicinity of Eureka. During the period between March 1 and 6 the values of sPV at 15, 17, 19 and 21 km were within the range between  $1.2 \times 10^{-4}$  and  $1.6 \times 10^{-4}$   $\text{s}^{-1}$  which approximately characterizes the location of outer and inner edge of the polar vortex correspondingly. Typically, the results of coincident measurements are compared to each other when the measurements are both conducted inside ( $\text{sPV} > 1.6 \times 10^{-4}$   $\text{s}^{-1}$ ) or outside ( $\text{sPV} < 1.2 \times 10^{-4}$   $\text{s}^{-1}$ ) the polar vortex. The measurements at the vortex edge are usually discarded from the comparisons since air mass characterization in such cases becomes challenging and utilization of traditional coincidence criteria based on close matching of time and location does not always provide good

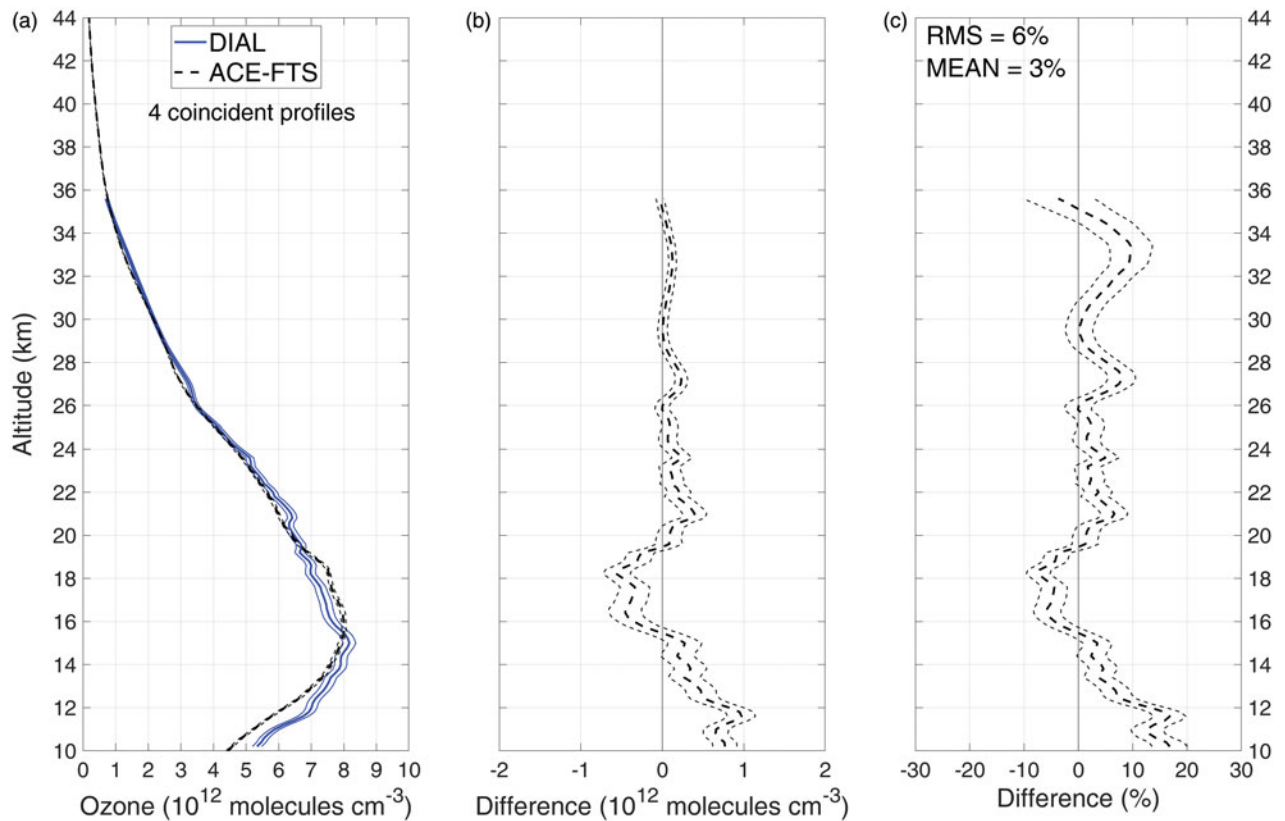


**Figure 8.** Mean ozone profiles and differences measured by DIAL and ACE-FTS, including all four coincident cases. (a) ozone number density. (b) absolute difference (DIAL - ACE-FTS). (c) the difference relative to ACE-FTS in percent:  $100 \times (\text{DIAL} - \text{ACE-FTS})/\text{ACE-FTS}$ . Dashed lines in subplot (a) for the DIAL represent random and systematic uncertainties summed in quadrature; for ACE-FTS - statistical error of ozone retrieval for each profile summed in quadrature. Dashed lines in subplots (b) and (c) depict the resultant uncertainty which is DIAL and ACE-FTS uncertainties summed in quadrature (see details in text).

correlation between the results of independent measurements. Similar but less strong than on March 3 negative laminae in the ozone concentration around 16 km–17 km in the ozonesonde profile is observed on February 9 (Figure 4 (a)), while on February 24 (Figure 4 (b)) a negative spike is observed around 11 km. On both dates the DIAL profiles remained smooth. According to MERRA2, sPV exhibited a rapid drop around February 9 and some fluctuations on February 24 indicating the passage of the polar vortex edge above Eureka (Figure 5 (b)). Our results are in agreement with Bird et al. (1997) and the references therein and show that the ozone can experience strong spatial and temporal inhomogeneities including presence of laminae in the vertical profiles in such unstable conditions when the edge of the polar vortex is located above the measurement site. This results in some discrepancy between coincident ozone profiles measured by different instruments with non-equal vertical resolution, particularly when temporal and spatial coincidence criteria cannot be precisely fulfilled.

According to MERRA2 on March 3 and 4 the polar vortex edge was located above Eureka and all

three instruments (DIAL, ozonesonde and OSIRIS) sensed the same air mass. The discrepancy in the profiles measured on March 3 by DIAL and ozonesonde can be explained by poorer vertical resolution of the DIAL in comparison with the ozonesonde and non-optimal temporal and spatial coincidence between the DIAL and the ozonesonde measurements. The discrepancy in the profiles measured on March 5 by DIAL, ozonesonde and OSIRIS is due to the fact that the instruments, according to MERRA2, sensed different air masses. The sPV values around 15 km altitude exhibited 30–50% variation within  $\pm 12$  hour period relatively to the time of nightly mean DIAL profile. Also non-optimal temporal and spatial coincidence between the measurements could affect the results in a way similar as it was suggested for March 3.

The performance of the DIAL has been also checked by comparing the DIAL to ozonesonde, ACE-FTS, ACE-MAESTRO and OSIRIS profiles averaged over all corresponding coincident cases (Figures 6–10). To equalize ozonesonde vertical resolution to the DIAL resolution, before taking the mean



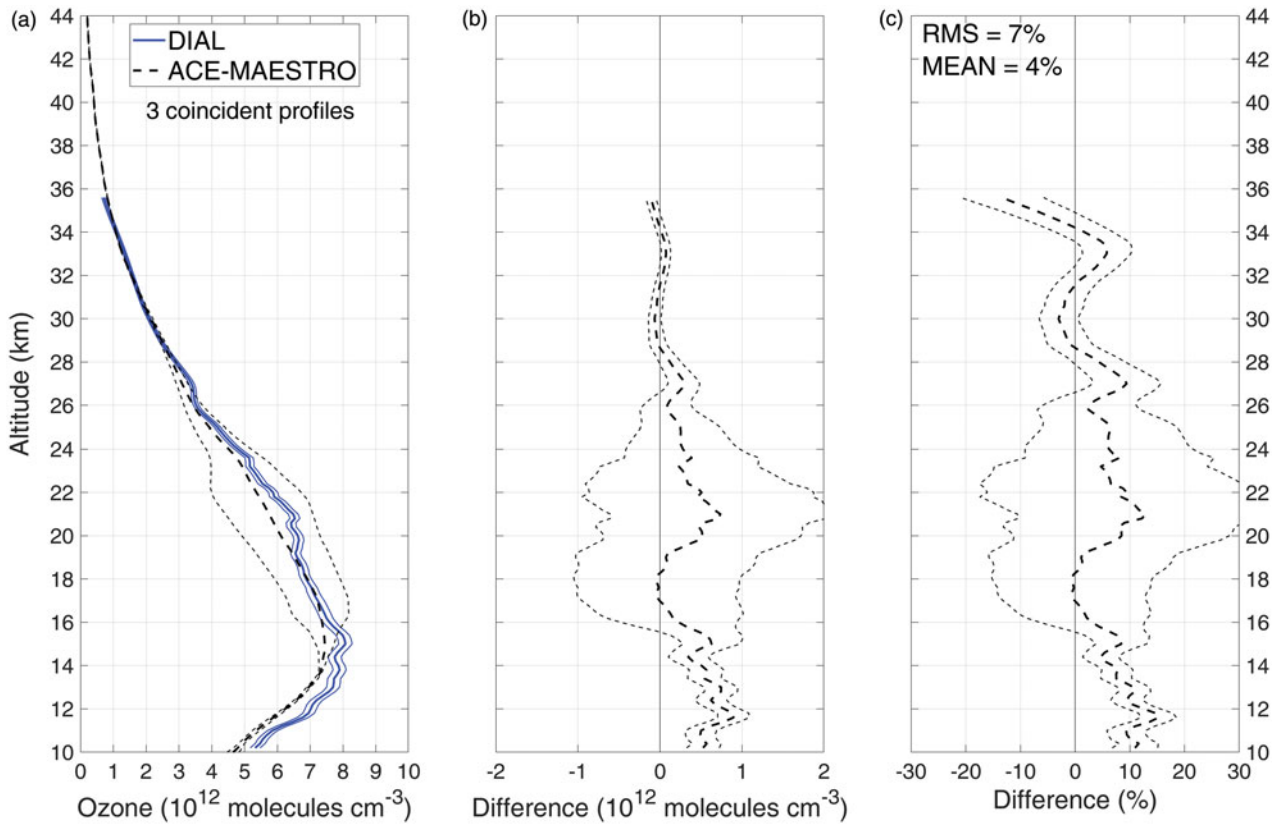


**Figure 9.** Mean ozone profiles and differences measured by DIAL and ACE-MAESTRO, including all three coincident cases. (a) ozone number density. (b) absolute difference (DIAL - ACE-MAESTRO). (c) the difference relative to ACE-MAESTRO in percent:  $100 \times (\text{DIAL} - \text{ACE-MAESTRO})/\text{ACE-MAESTRO}$ . Dashed lines in subplot (a) for the DIAL represent random and systematic uncertainties summed in quadrature; for ACE-MAESTRO - an uncertainty associated with a random error due to instrument noise propagated through the spectral fitting and vertical profile retrieval code. Dashed lines in subplots (b) and (c) depict the resultant uncertainty which is DIAL and ACE-MAESTRO uncertainties summed in quadrature (see details in text).

all ozonesonde profiles have been smoothed using moving average approach taking into account DIAL vertical resolution dependence on the altitude. As can be seen from Figure 6, the DIAL overestimates the ozone by about 10% on average between 10 km and 20 km altitude range in comparison with ozonesonde. We associate this overestimation with the discrepancy between coincident DIAL and ozonesonde profiles on March 3 and 5 which impacted the mean profile. Above 20 km altitude the agreement between the DIAL and the ozonesonde is within 10%. The root mean square (RMS in Figures 6–10) and arithmetic mean (MEAN) of the difference does not exceed 8 and 5% correspondingly for 10 km–30 km altitude range. If the coincident DIAL-ozonesonde profiles measured on March 3 and 5 are removed from the analysis the agreement between DIAL and ozonesonde is improved, i.e. the profiles agree with each other within 10–15% along the entire altitude range between 10 km and 30 km with RMS and MEAN of the difference equal to 4 and 0% (Figure 7). Coincident mean

ozone DIAL and ACE-FTS profiles agree with each other within 10% in the 12 km–36 km altitude range (Figure 8). However, up to 15% overestimation of the ozone is observed below 12 km by the DIAL in comparison with ACE-FTS. The RMS and MEAN of the difference is equal to 6 and 3%, respectively. The mean DIAL ozone profile is about 12% larger than ACE-MAESTRO profile below 12 km, which is close to ACE-FTS results, and as much as 15% larger than ACE-MAESTRO one around 21 km (Figure 9). Large values of the resultant uncertainty observed in the mean ACE-MAESTRO profile between 16 km and 26 km is due to the strong random noise which impacted ACE-MAESTRO retrieval on February 28 (see Figure 4 (f)). The RMS and MEAN values of the relative difference for the DIAL and ACE-MAESTRO comparison with 7 and 14%, correspondingly. The OSIRIS mean profile agrees within 10% with DIAL profile in the range between 15 km to 41 km with RMS and MEAN of the difference equal to 4 and 0%, respectively (Figure 10).

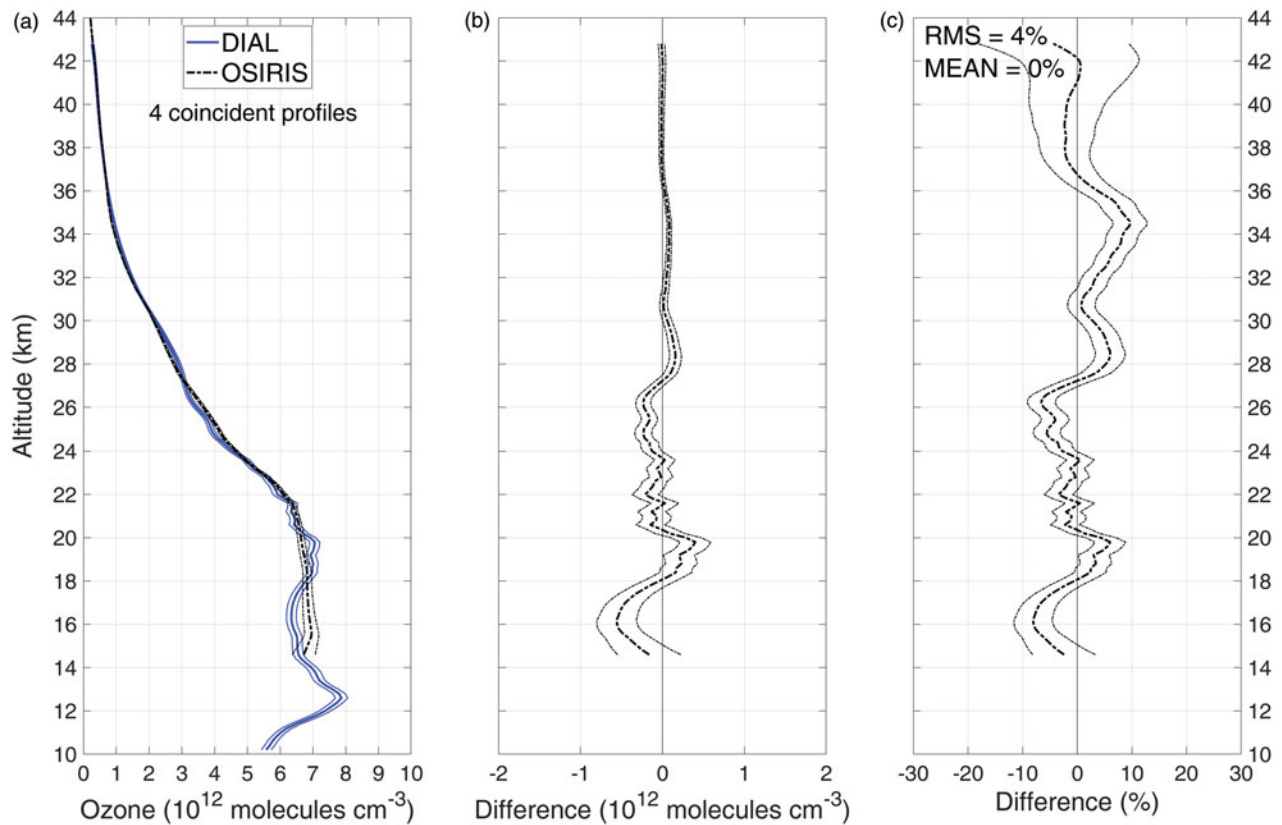


**Figure 10.** Mean ozone profiles and differences measured by DIAL and OSIRIS, including all three coincident cases. (a) ozone number density. (b) absolute difference (DIAL - OSIRIS). (c) the difference relative to OSIRIS in percent:  $100 \times (\text{DIAL} - \text{OSIRIS})/\text{OSIRIS}$ . Dashed lines in subplot (a) for the DIAL represent random and systematic uncertainties summed in quadrature; for OSIRIS - standard uncertainty of ozone concentration for each profile summed in quadrature. Dashed lines in subplots (b) and (c) depict the resultant uncertainty which is DIAL and OSIRIS uncertainties summed in quadrature (see details in text).

## Conclusion

Eureka stratospheric ozone DIAL is a powerful tool to measure vertical ozone distributions in the Canadian High Arctic. Between 2009 and 2015 the DIAL underwent an upgrade which included the laser, optical chopper, data acquisition system, secondary optics and servo control system, and control software. After the upgrade the instrument participated in the 2017 Canadian Arctic ACE/OSIRIS Validation Campaign and measured nightly mean vertical profiles of the ozone number density in the 10 km–45 km altitude range. DIAL vertical profiles have been compared to the measurements from the ozonesondes, launched at Eureka Weather Station, located 12 km from the DIAL site as well as to the ozone profiles obtained from ACE-FTS, ACE-MAESTRO and OSIRIS satellite instruments. DIAL profiles are in a good agreement with ozonesonde and satellite instrument profiles through most of the cases. The obtained results indicate satisfactory performance of the DIAL after its upgrade. Between March 3 and 5, 2017 a stratospheric ozone depletion event was seen by the DIAL,

ozonesonde and OSIRIS. During the depletion peak on March 3 the ozone number density dropped down to  $1 \times 10^{12}$  molecules  $\text{cm}^{-3}$  around 15.5 km as measured by the ozonesonde and below  $6 \times 10^{12}$  molecules  $\text{cm}^{-3}$  at 16 km as measured by the DIAL, which resulted in more than 50% overestimation of the ozone number density by the DIAL in comparison with the ozonesonde. The comparison of the DIAL and ozonesonde profiles, averaged over six coincident cases, shows the DIAL overestimates the ozone by about 10% between 10 and 20 km altitude range. This overestimation is associated with the discrepancy between the DIAL and ozonesonde profiles measured during the depletion on March 3 and 5. Above 20 km altitude the mean DIAL profile agrees to the mean ozonesonde profile within 10%. The discrepancy in the DIAL and ozonesonde profiles measured on March 3 and 5 is explained by poorer vertical resolution of the DIAL in comparison with the ozonesonde, non-optimal temporal and spatial coincidence between the measurements as well as by the fact that on March 5 the instruments sensed slightly different

air masses. If the cases on March 3 and 5 are removed from the comparison, the agreement between DIAL and ozonesonde is improved, i.e., the profiles agree with each other within 10–15% along the entire altitude range between 10 km and 30 km. For better DIAL-ozonesonde validation the smallest time difference between the DIAL and ozonesonde measurements is required. This can be accomplished by more coordinated ozonesonde launches. DIAL and ACE-FTS profiles agree within 10% to each other between 12 km and 36 km altitudes, but up to 15% overestimation of the ozone is observed below 12 km by the DIAL. The mean DIAL ozone is about 12% larger below 12 km and as much as 15% larger around 21 km than ACE-MAESTRO ozone. The OSIRIS ozone agrees within 10% with DIAL ozone over the entire altitude range between 15 km to 41 km.

Our comparisons here are in between those given by Steinbrecht (1994) and Donovan et al. (1995). Steinbrecht (1994) reported 10–20% DIAL-ozonesonde agreement in the 18 km to 34 km altitude region, while Donovan et al. (1995) found less than 7% average difference between the DIAL and ozonesonde measurements in the 11 km–22 km altitude range. Our results agree with Bird et al. (1997) and show that the ozone experiences strong spatial and temporal inhomogeneities including presence of laminated structures in the vertical profiles near the vortex edge regions. This results in some discrepancy between coincident ozone profiles measured by different instruments, particularly when temporal and spatial coincidence criteria cannot be precisely fulfilled.

For comparisons between DIAL and satellite instruments our results are close to Kerzenmacher et al. (2005) who showed 10% agreement in the 10 km–45 km altitude range between DIAL and ACE-FTS and better than reported by Dupuy et al. (2009) who found that DIAL overestimates both ACE-FTS and ACE-MAESTRO by about 7% based on 10 coincident measurements. We have not found any comparisons between DIAL and OSIRIS in the literature.

This is the first validation of the instrument after its upgrade. Our initial comparisons are encouraging and suggest both the new transmitter and upgraded control and data acquisition system are performing satisfactorily, and the Eureka Stratospheric Ozone DIAL can now be considered fully operational. To further improve the accuracy of validations the comparisons have to be carried out for the measurements located well inside or outside the polar vortex rather than for those on the vortex edge. However, this remains challenging due to the lack suitable cases.

Since 2017 the typical operation schedule of the DIAL has included from four to six weeks of ozone measurements in January–March and from 2 to 4 weeks in October–November each year. The DIAL group is working on improving of the DIAL control software and hardware to enable complete remote operation of the lidar from outside of Eureka to increase the instrument's up time. The DIAL group is always open for collaboration. The DIAL measurements can be requested via the PEARL principal investigator. Details can be found at CANDAC (2019).

### Data availability

DIAL and UT-GBS data used in this paper are available on-line at NDACC (2019) data archive. Ozonesonde and Brewer data are provided by ECCC and available on-line at the WOUDC. ACE-FTS and ACE-MAESTRO data products are available on request via ACE (2019) web page. OSIRIS data products are available in free access at the web page of the University of Saskatchewan Atmospheric Research Group (2019).

### Acknowledgements

Authors thank J. Davies, V. Fioletov and A. Ogyu (ECCC) for providing ozonesonde and Brewer data. They also thank DIAL laser installation team members M. Brohart, B. Firanski, M. Okraszewski and B. Anderson. In addition, the authors would like to acknowledge the following groups and individuals for their technical support during field campaigns in Eureka: Canadian Arctic ACE/OSIRIS Validation Campaign project lead K. A. Walker, CANDAC operators: J. Gallagher, A. Harrett, A. Khmel, P. Loewen, K. MacQuarrie, M. Maurice, P. McGovern, and O. Mikhailov; CANDAC data manager Y. Tsehtik. Authors thank the Eureka Weather Station staff for launching radio- and ozonesondes and operation support. Authors acknowledge A. Carswell, A. Ulitsky, S. Pal, T.-Y. Wang, M. Flood, K. Strawbridge and the developers of the original Eureka DIAL system from Optech Inc., Institute for Space and Terrestrial Science, York University and ECCC. A. B. Tikhomirov gratefully acknowledges the help he received from W. Steinbrecht and T. Duck in regards to the DIAL hardware and operation. He also thanks G. Lesins and C. Perro for fruitful discussions of the results. The assistance received from P. LaRocque and J. Hahn is greatly appreciated as well. A. B. Tikhomirov acknowledges A. Franzen for developing the ComponentLibrary. The library was used to draw the optical diagrams of the DIAL.

### Disclosure statement

The authors declare that they have no competing interests.

## Author contributions

Alexey B. Tikhomirov refurbished, upgraded and maintained the DIAL, developed new hardware and software for the DIAL, made measurements during the campaign, performed data quality control and analysis, contributed text and figures to the manuscript. Ghazal Farhani made measurements during the campaign, contributed text to the manuscript. Emily McCullough helped with installation of the new laser, carried out initial characterization of the old receiver with the new laser, analyzed context measurements, and contributed text to the manuscript. Pierre Fogal is PEARL site manager, provided logistics service, repaired and maintained DIAL laser during the campaign. Thierry Leblanc developed the code and carried out analysis of the DIAL data using the traditional ozone retrieval method. Robert J. Sica was the DIAL instrument mentor and supervised Farhani's graduate work. James R. Drummond was the Principal Investigator for the PEARL, developed new hardware for the DIAL and facilitated the upgrade and operations of the instrument.

## Funding

PEARL research is supported by: the Canadian Foundation for Innovation; the Ontario Innovation Trust; the Ontario Ministry of Research and Innovation; the Nova Scotia Research and Innovation Trust; the Natural Sciences and Engineering Research Council (NSERC); the Canadian Foundation for Climate and Atmospheric Science; Environment and Climate Change Canada (ECCC); Polar Continental Shelf Project; the Department of Indigenous and Northern Affairs Canada; and the Canadian Space Agency (CSA). This work was carried out during the 2017 Canadian Arctic ACE/OSIRIS Validation Campaign, which was funded by: CSA, ECCC, NSERC, and the Northern Scientific Training Program. This particular project has also been supported by NSERC Discovery Grants and Northern Supplement Grants held by J. R. Drummond, R. J. Sica, and K. A. Walker, and the NSERC CREATE Training Program in Arctic Atmospheric Science (PI: K. Strong). Part of this work has been carried out at the Jet Propulsion Laboratory, California Institute of Technology, under agreements with the National Aeronautics and Space Administration.

## ORCID

Robert J. Sica  <http://orcid.org/0000-0002-0598-5537>

## References

- ACE. 2019. "ACE Level 2 data product." Available at <http://www.ace.uwaterloo.ca>. Accessed Jan 5, 2019.
- Adams, C., Strong, K., Batchelor, R.L., Bernath, P.F., Brohede, S., Boone, C., Degenstein, D., et al. 2012. "Validation of ACE and OSIRIS Ozone and NO<sub>2</sub> Measurements Using Ground-Based Instruments at 80° N." *Atmospheric Measurement Techniques*, Vol. 5(No. 5): pp. 927–953. doi:10.5194/amt-5-927-2012.
- Ball, W.T., Alsing, J., Mortlock, D.J., Staehelin, J., Haigh, J.D., Peter, T., Tummon, F., et al. 2018. "Evidence for a Continuous Decline in Lower Stratospheric Ozone Offsetting Ozone Layer Recovery." *Atmospheric Chemistry and Physics*, Vol. 18(No. 2): pp. 1379–1394. doi:10.5194/acp-18-1379-2018.
- Bernath, P.F., McElroy, C.T., Abrams, M.C., Boone, C.D., Butler, M., Camy-Peyret, C., Carleer, M., et al. 2005. "Atmospheric Chemistry Experiment (ACE): Mission overview." *Geophysical Research Letters*, Vol. 32(No. 15): pp. 1–5. doi:10.1029/2005GL022386.
- Bird, J.C., Pal, S.R., Carswell, A.I., Donovan, D.P., Manney, G.L., Harris, J.M., and Uchino, O. 1997. "Observations of Ozone Structures in the Arctic Polar Vortex." *Journal of Geophysical Research: Atmospheres*, Vol. 102(No. D9): pp. 10785–10800. doi:10.1029/96JD03787.
- CANDAC. 2019. URL <http://www.candac.ca>. Accessed Jan 5, 2019.
- Carswell, A.I., Pal, S.R., Steinbrecht, W., Whiteway, J.A., Ulitsky, A., and Wang, T.Y. 1991. "Lidar Measurements of the Middle Atmosphere." *Canadian Journal of Physics*, Vol. 69(No. 8–9): pp. 1076–1086. doi:10.1139/p91-166.
- Carswell, A.I., Ulitsky, A., and Wardle, D.I. 1993. "Lidar Measurements of the Arctic Stratosphere." *Proc.SPIE*, Vol. 2049: pp. 9–23. doi:10.1117/12.163507.
- Chipperfield, M.P., Dhomse, S., Hossaini, R., Feng, W., Santee, M.L., Weber, M., Burrows, J.P., Wild, J.D., Loyola, D., and Coldewey-Egbers, M. 2018. "On the Cause of Recent Variations in Lower Stratospheric Ozone." *Geophysical Research Letters*, Vol. 45(No. 11): pp. 5718–5726. doi:10.1029/2018GL078071.
- Chubachi, S., and Kajiwara, R. 1986. "Total Ozone Variations at Syowa, Antarctica." *Geophysical Research Letters*, Vol. 13(No. 12): pp. 1197–1198. doi:10.1029/GL013i012p01197.
- Davies, J., Tarasick, D. W., McElroy, C. T., Kerr, J. B., Fogal, P. F., and Savastouk, V. 2007. "Evaluation of ECC Ozone Sonde Preparation Methods from Laboratory Tests and Field Comparisons during MANTRA," In *Proceedings of the Quadrennial Ozone Symposium*, edited by R. D. Bojkov, and S. Kazuo, pp. 137–138.
- Donovan, D.P., Bird, J.C., Whiteway, J.A., Duck, T.J., Pal, S.R., and Carswell, A.I. 1995. "Lidar Observations of Stratospheric Ozone and Aerosol above the Canadian High Arctic during the 1994–95 Winter." *Geophysical Research Letters*, Vol. 22(No. 24): pp. 3489–3492. doi:10.1029/95GL03337.
- Donovan, D.P., Fast, H., Makino, Y., Bird, J.C., Carswell, A.I., Davies, J., Duck, T.J., et al. 1997. "Ozone, Column ClO, and PSC Measurements made at the NDSC Eureka Observatory (80°N, 86°W) during the Spring of 1997." *Geophysical Research Letters*, Vol. 24(No. 22): pp. 2709–2712. doi:10.1029/97GL52828.
- Duck, T.J., and Whiteway, J.A. 2005. "The Spectrum of Waves and Turbulence at the Tropopause." *Geophysical Research Letters*, Vol. 32(No. 7): pp. L07801. doi:10.1029/2004GL021189.
- Duck, T.J., Whiteway, J.A., and Carswell, A.I. 1998. "Lidar Observations of Gravity wave Activity and Arctic Stratospheric Vortex Core Warming." *Geophysical Research Letters*, Vol. 25(No. 15): pp. 2813–2816. doi:10.1029/98GL02113.
- Duck, T.J., Whiteway, J.A., and Carswell, A.I. 2000. "A Detailed Record of High Arctic Middle Atmosphere

- Temperatures.” *Journal of Geophysical Research: Atmospheres*, Vol. 105(No. D18): pp. 22909–22918. doi:10.1029/2000JD900367.
- Duck, T.J., Whiteway, J.A., and Carswell, A.I. 2001. “The Gravity Wave-Arctic Stratospheric Vortex Interaction, American Meteorological Society.” *Journal of the Atmospheric Sciences*, Vol. 58: pp. 3581–3596. doi:10.1175/1520-0469(2001)058<3581:TGWASV>2.0.CO;2.
- Duck, T. 1999. High Arctic Observations of Strato-mesospheric Temperatures and Gravity Wave Activity, Ph.D. thesis, York University, Canada.
- Dunkerton, T.J., and Delisi, D.P. 1986. “Evolution of Potential Vorticity in the Winter Stratosphere of January-February 1979.” *Journal of Geophysical Research*, Vol. 91(No. D1): pp. 1199–1208. doi:10.1029/JD091iD01p01199.
- Dupuy, E., Walker, K.A., Kar, J., Boone, C.D., McElroy, C.T., Bernath, P.F., Drummond, J.R., et al. 2009. “Validation of Ozone Measurements from the Atmospheric Chemistry Experiment (ACE).” *Atmospheric Chemistry and Physics*, Vol. 9(No. 2): pp. 287–343. doi:10.5194/acp-9-287-2009.
- Farman, J.C., Gardiner, B.G., and Shanklin, J.D. 1985. “Large losses of total ozone in Antarctica Reveal Seasonal ClO<sub>x</sub>/NO<sub>x</sub> Interaction.” *Nature*, Vol. 315(No. 6016): pp. 207–210. doi:10.1038/315207a0.
- Fioletov, V.E., Kerr, J.B., McElroy, C.T., Wardle, D.I., Savastiouk, V., and Grajnar, T. S. 2005. “The Brewer Reference Triad.” *Geophysical Research Letters*, Vol. 32(No. 20): pp. L20805. doi:10.1029/2005GL024244.
- Fogal, P., LeBlanc, L., and Drummond, J. 2013. “The Polar Environment Atmospheric Research Laboratory (PEARL): Sounding the Atmosphere at 80° North.” *ARCTIC*, Vol. 66(No. 3): pp. 377–386. doi:10.14430/arctic4321.
- Fraser, A., Goutail, F., Strong, K., Bernath, P.F., Boone, C., Daffer, W.H., Drummond, J.R., et al. 2008. “Intercomparison of UV-Visible Measurements of Ozone and NO<sub>2</sub> during the Canadian Arctic ACE Validation Campaigns: 2004–2006.” *Atmospheric Chemistry and Physics*, Vol. 8(No. 6): pp. 1763–1788. doi:10.5194/acp-8-1763-2008.
- GEOS-5.12.4. 2019. JPL: “Daily Meteorological Plots.” Available at [https://mlls.jpl.nasa.gov/plots/met/met\\_plot\\_locator.php](https://mlls.jpl.nasa.gov/plots/met/met_plot_locator.php). Accessed Jan 5, 2019.
- Godin-Beekmann, S., Porteneuve, J., and Garnier, A. 2003. “Systematic DIAL Lidar Monitoring of the Stratospheric Ozone Vertical Distribution at Observatoire de Haute-Provence (43.92 degrees N, 5.71 degrees E).” *Journal of Environmental Monitoring: JEM*, Vol. 5(No. 1): pp. 57–67.
- Griffin, D., Walker, K.A., Conway, S., Kolonjari, F., Strong, K., Batchelor, R., Boone, C.D., et al. 2017. “Multi-Year Comparisons of Ground-Based and Space-Borne Fourier Transform Spectrometers in the High Arctic between 2006 and 2013.” *Atmospheric Measurement Techniques*, Vol. 10(No. 9): pp. 3273–3294. doi:10.5194/amt-10-3273-2017.
- JCGM. 2008a. International vocabulary of basic and general terms in metrology (VIM), Tech. Rep. JCGM 200:2008, International Bureau of Weights and Measures (BIPM).
- JCGM. 2008b. Evaluation of measurement data – Guide to the expression of uncertainty in measurement (GUM), Tech. Rep. JCGM 100:2008, International Bureau of Weights and Measures (BIPM).
- JCGM. 2009. Evaluation of measurement data - An introduction to the Guide to the expression of uncertainty in measurement and related documents, Tech. Rep. JCGM 104: 2009, International Bureau of Weights and Measures (BIPM).
- JCGM. 2012. International Vocabulary of Metrology – Basic and General Concepts and Associated Terms (VIM3), Tech. Rep. JCGM 200:2012, International Bureau of Weights and Measures (BIPM).
- Jones, A., Urban, J., Murtagh, D.P., Eriksson, P., Brohede, S., Haley, C., Degenstein, D., et al. 2009. “Evolution of Stratospheric Ozone and Water Vapour Time Series Studied with Satellite Measurements.” *Atmospheric Chemistry and Physics*, Vol. 9(No. 16): pp. 6055–6075. doi:10.5194/acp-9-6055-2009.
- Kerzenmacher, T.E., Walker, K.A., Strong, K., Berman, R., Bernath, P.F., Boone, C.D., Drummond, J.R., et al. 2005. “Measurements of O<sub>3</sub>, NO<sub>2</sub> and Temperature during the 2004 Canadian Arctic ACE Validation Campaign.” *Geophysical Research Letters*, Vol. 32(No. 16): pp. 1–5.
- Krizan, P., Lastovicka, J., and Kozubek, M. 2015. “Size Dependence of Ozone Lamina Characteristics and their Correlations.” *Journal of Atmospheric and Solar-Terrestrial Physics*, Vol. 132: pp. 116–123. doi:10.1016/j.jastp.2015.06.017.
- Leblanc, T., Sica, R.J., van Gijssel, J.A.E., Godin-Beekmann, S., Haefele, A., Trickl, T., Payen, G., and Gabarrot, F. 2016a. “Proposed Standardized Definitions for Vertical Resolution and Uncertainty in the NDACC Lidar Ozone and Temperature Algorithms – Part 1: Vertical Resolution.” *Atmospheric Measurement Techniques*, Vol. 9(No. 8): pp. 4029–4049. doi:10.5194/amt-9-4029-2016.
- Leblanc, T., Sica, R.J., van Gijssel, J.A.E., Godin-Beekmann, S., Haefele, A., Trickl, T., Payen, G., and Liberti, G. 2016b. “Proposed Standardized Definitions for Vertical Resolution and Uncertainty in the NDACC Lidar Ozone and Temperature Algorithms – Part 2: Ozone DIAL Uncertainty Budget.” *Atmospheric Measurement Techniques*, Vol. 9(No. 8): pp. 4051–4078. doi:10.5194/amt-9-4051-2016.
- Lindenmaier, R., Strong, K., Batchelor, R.L., Chipperfield, M.P., Daffer, W.H., Drummond, J.R., Duck, T.J., et al. 2012. “Unusually Low Ozone, HCl, and HNO<sub>3</sub> Column Measurements at Eureka, Canada during Winter/Spring 2011.” *Atmospheric Chemistry and Physics*, Vol. 12(No. 8): pp. 3821–3835. doi:10.5194/acp-12-3821-2012.
- Llewellyn, E.J., Lloyd, N.D., Degenstein, D.A., Gattinger, R.L., Petelina, S.V., Bourassa, A.E., Wiens, J.T., et al. 2004. “The OSIRIS Instrument on the Odin Spacecraft.” *Canadian Journal of Physics*, Vol. 82(No. 6): pp. 411–422. doi:10.1139/p04-005.
- Manney, G.L., Santee, M.L., Rex, M., Livesey, N.J., Pitts, M.C., Veefkind, P., Nash, E.R., et al. 2011. “Unprecedented Arctic Ozone Loss in 2011.” *Nature*, Vol. 478(No. 7370): pp. 469–475. doi:10.1038/nature10556.
- Manney, G.L., Zurek, R.W., O’Neill, A., and Swinbank, R. 1994. “On the Motion of Air through the Stratospheric Polar Vortex.” *Journal of the Atmospheric Sciences*, Vol. 51(No. 20): pp. 2973–2994. doi:10.1175/1520-0469(1994)051<2973:OTMOAT>2.0.CO;2.

- McElroy, C.T., Nowlan, C.R., Drummond, J.R., Bernath, P.F., Barton, D.V., Dufour, D.G., Midwinter, C., et al. 2007. "The ACE-MAESTRO Instrument on SCISAT: Description, Performance, and Preliminary Results." *Applied Optics*, Vol. 46(No. 20): pp. 4341–4356. doi:10.1364/AO.46.004341.
- Megie, G., Allain, J.Y., Chanin, M.L., and Blamont, J.E. 1977. "Vertical Profile of Stratospheric Ozone by Lidar Sounding from the Ground." *Nature*, Vol. 270: pp. 329–331. doi:10.1038/270329a0.
- Montzka, S.A., Dutton, G.S., Yu, P., Ray, E., Portmann, R.W., Daniel, J.S., Kuijpers, L., et al. 2018. "An Unexpected and Persistent Increase in Global Emissions of Ozone-Depleting CFC-11." *Nature*, Vol. 557(No. 7705): pp. 413–417. doi:10.1038/s41586-018-0106-2.
- Moss, A., Sica, R., McCullough, E., Strawbridge, K., Walker, K., and Drummond, J. 2012. "Calibration and Validation of Water Vapour Lidar Measurements from Eureka, Nunavut using Radiosondes and the Atmospheric Chemistry Experiment Fourier Transform Spectrometer." *Atmospheric Measurement Techniques Discussions*, Vol. 5(No. 4): pp. 5665–5689. doi:10.5194/amtd-5-5665-2012.
- NASA. 2019. "MERRA2 Data Products." Available at <https://goldsmr5.gesdisc.eosdis.nasa.gov/data/MERRA2/M2I3NPASM.5.12.4/>. Accessed Jan 5, 2019.
- NDACC. 2019. URL <http://www.ndsc.ncep.noaa.gov>. Accessed Jan 5, 2019.
- Pal, S.R., Carswell, A.I., John, B., Donovan, D.P., Duck, T., and Whiteway, J. 1996. "Lidar Measurements of the Stratosphere at the Eureka and Toronto NDSC Stations." *Proc.SPIE*, Vol. 2833: pp. 28–39. doi:10.1117/12.258164.
- Schotland, R. M. 1964. The Determination of the Vertical Profile of Atmospheric Gases by Means of a Ground-Based Optical Radar, in: in Proceedings, Third Symposium on Remote Sensing of the Environment (Environmental Research Institute of Michigan, Ann Arbor).
- Schotland, R.M. 1974. "Errors in the Lidar Measurement of Atmospheric Gases by Differential Absorption." *Journal of Applied Meteorology (1962–1982)*, Vol. 13: pp. 71–77. URL <http://www.jstor.org/stable/26176876>.
- Steinbrecht, W., Froidevaux, L., Fuller, R., Wang, R., Anderson, J., Roth, C., Bourassa, A., et al. 2017. "An Update on Ozone Profile Trends for the Period 2000 to 2016." *Atmospheric Chemistry and Physics*, Vol. 17(No. 17): pp. 10675–10690. doi:10.5194/acp-17-10675-2017.
- Steinbrecht, W. 1994. LIDAR Measurements of Ozone, Aerosol and Temperature in the Stratosphere, Ph.D. thesis, York University, Canada.
- Tarasick, D.W., Fioletov, V.E., Wardle, D.I., Kerr, J.B., and Davies, J. 2005. "Changes in the Vertical Distribution of Ozone over Canada from Ozonesondes: 1980–2001." *Journal of Geophysical Research*, Vol. 110(No. D2): pp. D02304. doi:10.1029/2004JD004643.
- Tummon, F., Hassler, B., Harris, N.R.P., Staehelin, J., Steinbrecht, W., Anderson, J., Bodeker, G.E., et al. 2015. "Intercomparison of Vertically Resolved Merged Satellite Ozone Data Sets: Interannual Variability and Long-Term Trends." *Atmospheric Chemistry and Physics*, Vol. 15(No. 6): pp. 3021–3043. doi: 10.5194/acp-15-3021-2015.
- UNEP. 2012. Handbook for the Montreal Protocol on Substances that Deplete the Ozone Layer, Secretariat for The Vienna Convention for the Protection of the Ozone Layer & The Montreal Protocol on Substances that Deplete the Ozone Layer, 9-th edn.
- University of Saskatchewan Atmospheric Research Group. 2019. "OSIRIS Level 2 data product." Available at <https://arg.usask.ca/projects/osiris/>. Accessed Jan 5, 2019.
- Whiteway, J.A., and Carswell, A.I. 1994. "Rayleigh Lidar Observations of the Thermal Structure and Gravity Wave Activity in the High Arctic during a Stratospheric Warming." *Journal of the Atmospheric Sciences*, Vol. 51(No. 21): pp. 3122. doi:10.1175/1520-0469(1994)051<3122:RLOOTS>2.0.CO;2.
- WMO. 2011. Scientific Assessment of Ozone Depletion: 2010, World Meteorological Organization, Global Ozone Research and Monitoring Project, Tech. Rep. No. 52, World Meteorological Organization.
- WMO. 2014. Scientific Assessment of Ozone Depletion: 2014, World Meteorological Organization, Global Ozone Research and Monitoring Project, Tech. Rep. No. 55, World Meteorological Organization.
- WOUDC. 2019. URL <https://woudc.org>. Accessed Jan 5, 2019.